样式定义: 公式: 字体: (默认) Cambria Math, (中文) +中文正文 (等线), 左, 行距: 1.5 倍行距

Reply to RC1

This study reported field measurements results of the chemical speciation, hygroscopicity and CCN properties of ambient particles at a suburban site in the central North China Plain (NCP). The probability density function of the hygroscopicity parameter kappa-PDF was then derived from measurement data and showed only a singular hygrophilic mode which was very different from profiles observed in other regions of the NCP (that were normally bi- or tri-modal). Among the possible factors affecting aerosol hygroscopicity (the mixing state, chemical composition and particle size), particle size was identified as the key factor influencing the particle CCN activation. This study explored the aerosol microphysical properties in a region that was not previously studied and the results can be useful when compared with existing data to understand aerosol aging and its impact on particle microphysics and the climate. The topic is relevant to the scope of the journal of Atmospheric Chemistry and Physics and should be considered for publication.

(1) The tile may be changed to "Characterization of aerosol hygroscopicity, mixing state, and CCN activity at a suburban site in the central North China Plain" to reflect the unique location of this study.
Re: It's a good suggestion, the title has been revised. Very thanks.

(2) Section 4.1, Lines 317-321: While it's been shown that aging of BC will enhance its hygroscopicity and CCN activation, the actual determination of the GF of aged BC could be challenging (see, for example, Torsten et al., Environ. Res. Lett., 2011) as the DMA mobility size change may be marginal. A few chambers studies on soot SOA from anthropogenic VOCs may provide some insights here (Guo et al., ES&T, 2016 and Qiu et al., ES&T, 2012). In general, the knowledge on particle morphology is useful, and in principle, ACSM and DMA data can be combine to retrieve morphology information.
Re: Thanks for your suggestion and the recommended references. We read the recommended papers carefully and indeed found a more comprehensive interpretation for the enhanced hygroscopicity. The lines have been revised as "This suggests that the particles were highly aged and internally mixed at XT during this campaign. Coating of sulfates and secondary organics during the aging process changes the structure of BC and makes it grow, which can significantly enhance the hygroscopicity of particles (e.g., Zhang et al., 2008; Jimenez et al., 2009; Tritscher et al., 2011; Guo et al., 2016).

(3) Section 4.1, Lines 347-351: As pointed out by recent studies, amines may contribute significantly to the NPF events (e.g., Zhang et al., Chem Rev., 2015). Several studies have shown that amine compounds in aerosol phase can be hygroscopic, sometimes even at event low RH (e.g., Gomez-Hernandez et al., ES&T, 2016; Chu et al., PCCP, 2015; Qiu and Zhang, ES&T, 2013). Since the

reported field measurements took place in a local with heavy industrial activities, it is possible that amine may contribute significantly to the hygroscopicity of the 40-nm particles

Re: This is a good point interpreting the hygroscopicity difference of 40 nm particles with other size particles. According to the recommended references, the lines have been revised as "40 nm particles were always more hygroscopic than 80 nm particles at XT, especially in the daytime, which was also different from other sites. This is likely because the coating effect of sulfates and secondary organics is more significant on smaller particles (Tritscher et al., 2011; Guo et al., 2016). Furthermore, since the field measurements took place in a local with heavy industrial activities, it is possible that amine contributes significantly to the hygroscopicity of 40 nm particles. Several studies have shown that amine compounds in aerosol phase can be hygroscopic, sometimes at even low RH (Qiu et al., 2012; Chu et al., 2015; Gomez-Hernandez et al., 2016).".

(4) Section 4.3: It would make more sense to merge Figures 6&7 as the discussions on the two figures are closely related.

Re: It's a good suggestion, we have merge them, as:

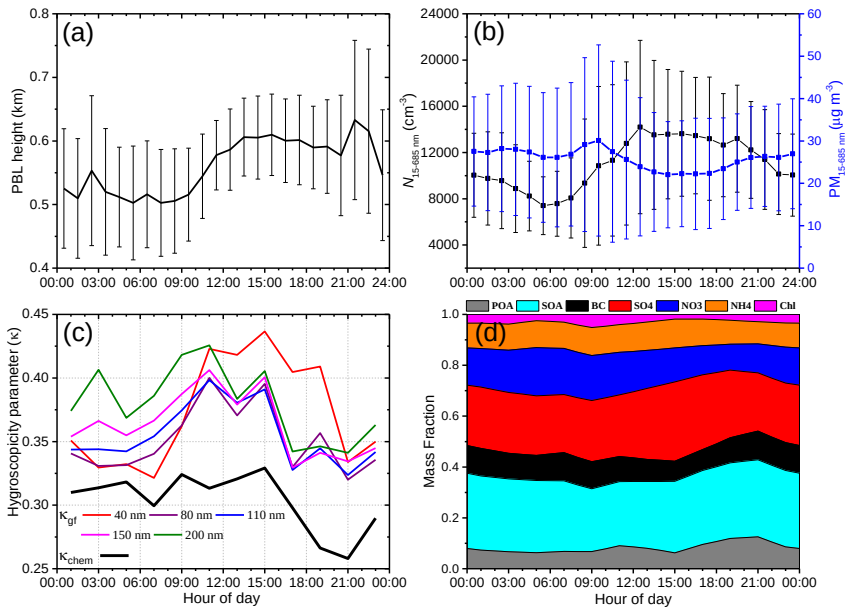

As the reviewer's suggestion, the merging make more sense. For example, we find the increase of hygroscopicity parameter (κ_{gf}) in the morning was synchronous with the particle number concentration ($N_{15\text{-}685\ nm}$), but was not with the PBL height, further suggesting the impact of photochemical reactions on aerosol hygroscopicity.

(5) Section 4.4: It seems odd that kappa was not derived from CCN data as described by Petters and Kreidenweis (2007). A side-by-side comparison of kappa values

derived from HTDMA, chemical speciation and CCN may be more straightforward. Also, CCNderived kappa values can also provide basis for comparison with other studies that may only had CCN results.

Re: Yes, we will obtain more information about aerosol hygroscopicity if kappa from CCN data can be derived. However, it needs to connect DMA and CCNc to measure the size-CCN number concentration. Unfortunately, we only measure the bulk CCN number concentration in the campaign. We will do the work in the future campaigns.

References:

Chu Y., Sauerwein M. and Chan C.K.: Hygroscopic and phase transition properties of alkyl aminium sulfates at low relative humidities, Phys Chem Chem Phys, 17, 19789-19796, https://doi.org/10.1039/c5cp02404h, 2015.

Gomez-Hernandez M., McKeown M., Secrest J., Marrero-Ortiz W., Lavi A., Rudich Y., Collins D.R. and Zhang R.: Hygroscopic Characteristics of Alkylaminium Carboxylate Aerosols, Environ Sci Technol, 50, 2292-2300, https://dx.doi.org/10.1021/acs.est.5b04691, 2016.

Guo S., Hu M., Lin Y., Gomez-Hernandez M., Zamora M.L., Peng J., Collins D.R. and Zhang R.: OH-Initiated Oxidation of m-Xylene on Black Carbon Aging, Environ Sci Technol, 50, 8605-8612, https://dx.doi.org/10.1021/acs.est.6b01272, 2016.

Qiu C. and Zhang R.: Physiochemical Properties of Alkylaminium Sulfates: Hygroscopicity, Thermostability, and Density, Environ Sci Technol, 46, 4474-4480, https://dx.doi.org/10.1021/es3004377, 2012.

Tritscher T., Juranyi Z., Martin M., Chirico R., Gysel M., Heringa M.F., DeCarlo P.F., Sierau B., Prevot A.S.H., Weingartner E. and Baltensperger U.: Changes of hygroscopicity and morphology during ageing of diesel soot, Environ. Res. Lett., 6, https://dx.doi.org/10.1088/1748-9326/6/3/034026, 2011.

Reply to RC2

Based on a field campaign conducted in Xingtai in the central North China Plain, the authors discussed about the chemical composition, hygroscopicity and CCN activity of aerosol particles. There have been a number of studies talked about the north part of NCP but very few about the central part. And it was found that aerosol mixing state and hygroscopicity in Xingtai largely differs from that in the north part of NCP. My major concerns are:

1) Xingtai locates at the western boundary of NCP and is heavily affected by the mountain-valley wind (L126). Can the measurement well represent the background aerosol in the central NCP?

Re: The influence of mountain-valley wind is regional. Figure 1 in this reply shows pollution in the NCP is rather non-uniform, the central region is more serious than that in northern and southern regions. Our sampling site (Xingtai) is located in one of the pollution centers and thus represents the condition near an emission source region. The average $PM_{2.5}$ mass concentration at this station was 45.2 μg m^{-3} in this campaign, which was only 15% lower than that (53.3 μg m^{-3}) measured at the urban site in Xingtai. In addition, OOA and sulfate were the most important organic and inorganic species respectively. Figure 2 in this reply shows that the diurnal cycle of OOA was flat and the diurnal cycle of sulfate was also smoother compared with nitrate, also reflecting the regional characteristics of the main pollutants. All these suggest that the influence of mountain-valley wind is limited and this site is a good representative in this region. Detailed discussion about gas precursors and aerosol chemical species in this region can be found in Zhang et al., (2018).

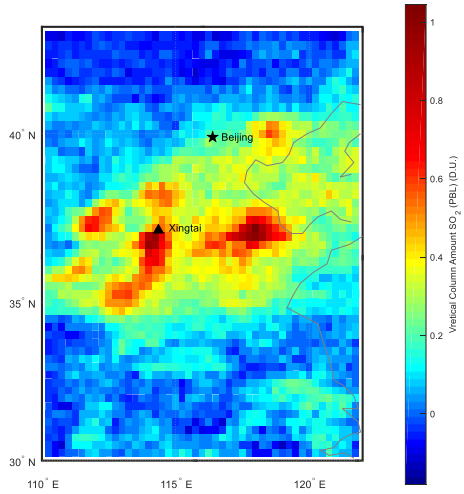

Figure 1. The distribution of mean SO_2 concentrations of May from 2012 to 2016. The map of NCP can refer to Fig. 4 in this reply.

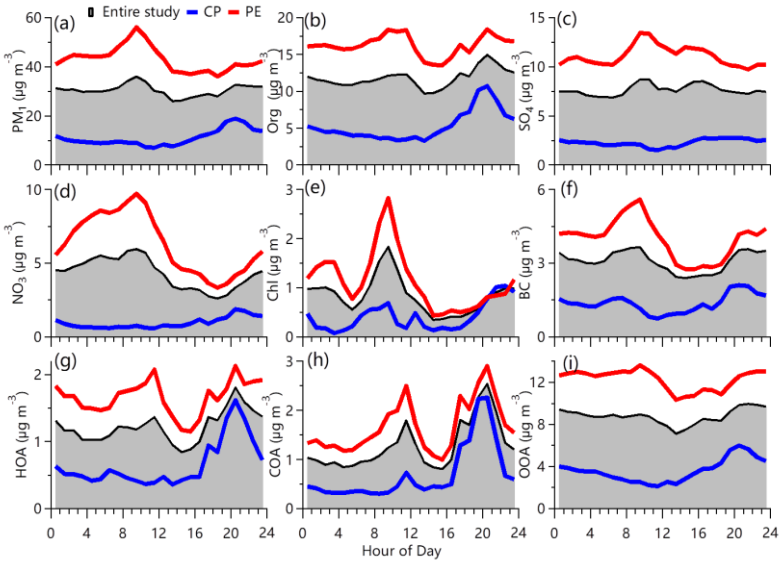

Figure 2. Diurnal cycles of chemical species of PM_1 and OA factors during entire study, PE (polluted events) and CP (clean periods). The figure is from Zhang et al., (2018).

2) I did not find a strong connection between the sections of CCN (section 4.3.3 and 4.4) and HTDMA (section 4.1 to 4.3.2). They look like two independent works but each of them a too weak to be an individual study.

Re: Aerosol mixing state is one of three factors influencing aerosol activation ability. In this campaign, we only measured bulk CCN data rather than size-resolved CCN data. The bulk CCN data cannot provide the information about aerosol mixing state but HTDMA data can. HTDMA data in this campaign suggests the aerosol is highly internal-mixed and aged, which is the base to do CCN closure studies in this paper. In addition, the HTDMA data are very useful for the analysis of the activation rate diurnal variations. These are important links between the sections of HTDMA and CCN.

Specific comments:

L51: defined as the mixture of solid and liquid particles suspended in air,

Re: Good suggestion, we have corrected.

L79: I did not see any causal relationship between L72-78 and L79-81

Re: L79-81 had been corrected as “aerosol hygroscopicity and CCN activity are very different in different regions due to different chemical compositions”.

L113: the author need to give more detailed information of the station. Does it locate in urban, sub-urban or rural environment? What about the surroundings, any roads, industrial or residential activities nearby?

Re: This suburban site is situated ~17 km northwest of Xingtai urban area in southern Hebei Province. A provincial road is ~400 m southeast of the sample site, a school adjoins the east, and a town is ~600 m in the northwest (Fig. 3 in this reply). There are many industrial manufacturers in this region including coal-based power plants, steel and iron works, glassworks, and cement mills. We have added more environment information about the sample site in the manuscript.

Figure **3**. The surroundings at the sample site.

L114: how do the authors define the NCP? From the map in Fig. 1 it seems the station locates at the southern boundary of the plain. In L126 the authors also state the station is "heavily affected by the mountain-valley wind".

Re: NCP is one of the largest plains in China. It covers an area of about 0.3 million square kilometers. The Fig.1 in the manuscript only shows a part of NCP, a full image can refer to Fig. 4 in this reply. This figure shows the observation site is in the central NCP although it is not far away from the Taihang Mountains. This station is still a good representative site in this region although it is affected by the mountain-valley wind (c.f. response to the Question 1).

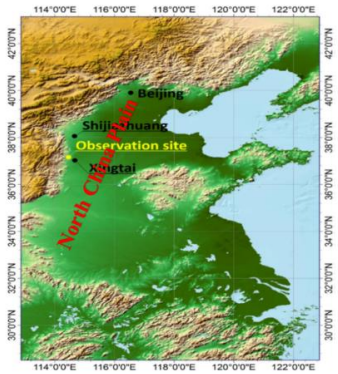

Figure **4**. Map showing the observation site and the scale of North China Plain (NCP). The original figure is from Wang et al., (2018).

L138: are then passed – pass

Re: Yes, we have corrected it.

L144: Normally the RH of the HTDMA should be calibrated with ammonium sulfate, especially for high RH measurement. Did the authors calibrate the system during the campaign?

Re: Yes, the RH calibration is important for HTDMA running. Figure 5 in this reply shows the calibration result with ammonium sulfate during our campaign. It shows the deliquescence point of ammonium sulfate is 78±1 %, this is consistent with previous studies (Badger et al., 2006; Tan et al., 2013).

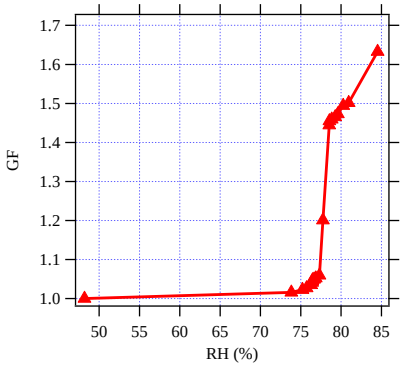

Figure **5**. Humidogram of ammonium sulfate for 150-nm particles measured with the HTDMA.

L147: I suggest to use single letter for variables, for example, f_{g} for growth factor.

Re: It's a good suggestion, but we tried to follow the conventional acronyms such as "GF" or "*gf*" that has been used in most previous papers. "f_g" is a good suggestion but it's easily confused with the expression of the aerosol scattering enhancement factor (f_{RH}). Therefore, we'd prefer to continue the use of "GF" in this manuscript.

L154: An Aerosol Chemical. . .

Re: Corrected per the comment.

L156: Is the cyclone for all the aerosol instruments or only for the ACSM?

Re: ACSM and AE33 had their separate cyclones. SMPS had an impactor in the inlet, which can also remove the most particles larger than its measurement range. HTDMA had no cyclone which has a minor effect on its measurement. CCNc had not also a cyclone because it needed to measure the bulk CCN number concentration in this campaign.

L164: Is there a separate inlet line with PM1 size cut for the aethalometer? I think the authors need to give a clear description of the inlets and sampling line for all the instruments. Now I am a bit confused.

Re: Yes, aethalometer had a separate inlet headed by a PM_1 for filtering particle size great than 1μm. CCNc and HTDMA shared the same inlet. During this campaign, all sampling instruments were placed in two containers at ground level and two air conditioners were used to maintain the temperature at 20–25 ^{o}C inside containers. All stainless tube inlets were 1.5 m above the top of containers.

L181: I do not know why the SS needs to be corrected. Normally after applying the calibration parameters to the system, the set SS is the true effective SS in the chamber. No more correction is needed. Is the SS corrected with the first or second calibration result? Is there any large difference between the two calibrations?

Re: Actually, the SS is influenced by flow rates and the temperature gradient in the cloud column. Therefore, the flow and temperature calibrations are also needed, which had been conducted before this campaign and the corresponding parameters were applied in the system. However, the SS maybe changed if the CCNc runs unsteadily, so we did two SS campaigns before and after the campaign instead of using the SS parameters from a single calibration. Figure 6 in this reply shows the results of the SS calibrations, the calibration method is the same as Rose et al., (2008). The results show CCNc run well and steadily during this campaign. The calibrated SS used in this paper was from the mean SS of two calibration results.

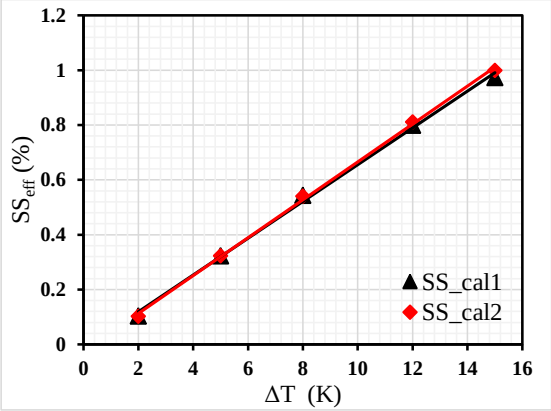

Figure **6**. The results of SS calibration experiments with ammonium sulfate: CCN efficiency spectra measured at 5 different temperature gradient (ΔT). SS_cal1 and SS_cal2 are the calibration results before and after the campaign respectively.

L183: AR defined in the manuscript is determined both on chemical composition and PNSD. I suggest using critical diameter.

Re: The critical diameter ($D_{0,crit}$) used in this study was derived from the hygroscopicity parameter (κ_{chem}), not measured directly. AR is used for a preliminary analysis of its relationships with nucleation events and PBL height. In the further campaigns, we will conduct the size-resolved CCN measurements through connecting DMA and CCNc. The critical diameter will be retrieved from size-CCN data, which can study the relationships in detail.

L235: I guess here the authors mean the kappa-Sc relationship.

Re: The relationships of κ, S_c ($S_c = s_c$ -1) and D_d is shown in Fig.1 in Petters et al. (2007). Actually, the D_d is the critical diameter corresponding to the critical supersaturation when κ is known. Therefore, here we first establish the s_c-D_d relationship, not κ-s_c relationship.

L246: How do the authors define the mean diameter.

Re: Here the mean diameter is the geometric mean diameter (D_m). It is defined as:

$$D_m = \frac{\int_{15nm}^{685nm} n(\log D_p) D_p \mathrm{d}\log D_p}{\int_{15nm}^{685nm} n(\log D_p) \mathrm{d}\log D_p}$$

We found a mistake in its calculation previously, now it has been corrected in the revised manuscript for which we are very grateful to the reviewer.

L261: Is there undefined species? Maybe the authors can do a simple mass closure between ACSM and SMPS data by assuming a typical aerosol density in that region, to check if there is anything missing in the aerosol mass defined by ACSM. This is important since the authors use this data later to estimate kappa.

Re: The mass closure between ACSM and SMPS is hard to realize because aerosol density and morphology are unknown during this campaign. Even so, we try to do a simple mass closure according to the suggestion of the reviewer. Here we assume aerosol particles are spherical and the density is 1.6 g/cm^3. The closure result (Fig. 8 in this reply) shows the two masses are related dependent on time. For most of the time, their correlation is good although the SMPS mass was always lower than that of ACSM+BC. The biases are likely caused by different measurement size range, and the variations of aerosol density and morphology.

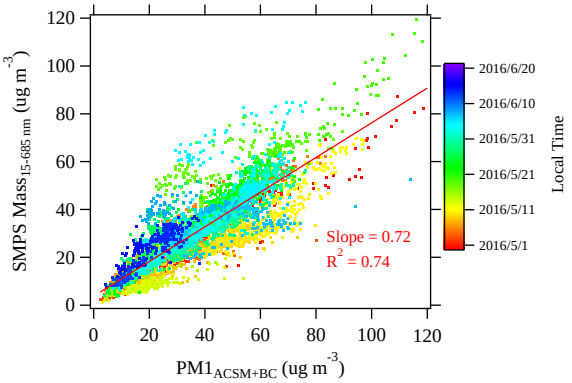

Figure **7**. Comparison of the mass concentrations of PM_1 (=NR-PM_1+BC) with those derived from SMPS measurements (D_p = 15-685 nm).

L267: How did the authors assume the kappa for HOA, SOA and OOA?

Re: The gravimetric densities (ρ) and hygroscopicity parameters (κ) of all species used in this study for CCN closure (note: POA = HOA+COA, SOA = OOA).

Species	NH_4NO_3	$(NH_4)_2SO_4$	NH_4HSO_4	H_2SO_4	POA	SOA	BC
ρ (kg m^{-3})	1720	1769	1780	1830	1000	1400	1700
K	0.67	0.61	0.61	0.9	0	0.1	0

L277: the hydrophobic mode locates at kappa of 0.05 for Dd of 40 nm, and shift towards 0 for large particles. Do the authors have any explanation on this?

Re: The direct comparison of the κ-PDF is depicted in Fig. 9 in this reply. There is an obvious difference of the hydrophobic mode as the reviewer found. This is related to the different chemical compositions. The hydrophobic mode of 40-nm particles is mainly caused by organics, while that of the larger particles is mainly caused by BC. BC is fully hydrophobic but some organics has a limited water uptake ability. This can be verified from previous studies, Wu et al., (2017) reported the fresh emitted BC are mainly in the accumulation mode.

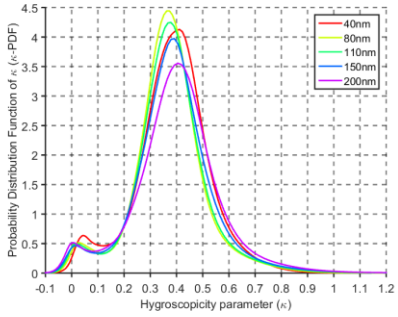

Figure 8. Comparison of κ-PDF of different size particles.

L305: the difference decreases with increasing size because most of the larger particles are well aged.

Re: Good point. We have added the corresponding expression.

L316: of precursors

Re: We have corrected.

L316: is there trace gas (SO2, NOx etc.) measurement during the campaign to support the hypothesis here?

Re: Yes. Figure 10 in this reply shows the diurnal variations of trace gases and meteorological variables (*T* and RH) in this campaign. Affected by the mountain-valley wind, prevailing winds shifted from the northwest to the southeast in the early morning. There are more industrial emissions to the southeast of the measurement site than to the northwest. Therefore, the CO, SO_2 concentrations increased sharply in the morning after the wind shift. The increased CO suggests the increase of VOCs because of their similar sources. The O_3 concentration increased gradually after sunrise during the day, reflecting the enhancement of atmospheric oxidation capacity. The ample supply of effluent SO_2 and VOCs precursors and the strong atmospheric oxidation capacity under high RH and low T conditions made plenty of sulfate and SOA produce (Wang et al., 2016; Wang et al., 2017). This is the reason in the frequent occurrence of NPF events and the enhancement of aerosol hygroscopicity during the daytime at XT.

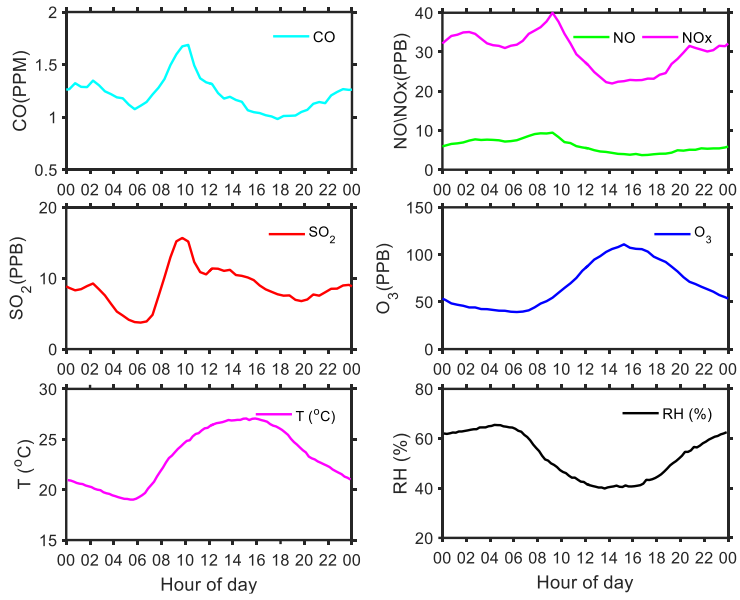

Figure **9**. Diurnal variations in trace gases (CO, NOx/NO, SO2 and O3) and meteorological variables (*T* and RH).

L346: 100 nm is too much for nucleation mode.

Re: It has been corrected as "small Aitken mode particles (< 50 nm)".

L359: From Fig. 6 it seems kappa already starts decrease at 12:00. The secondary aerosol production is also active in the afternoon (Fig. 7b). Why does kappa for larger particles decrease?

Re: This is related with the local emissions, especially the emitted organics. As is shown in the diurnal variations (Fig.2 in this reply), the primary organics (COA and HOA) increase sharply near noon. This is the reason why κ has a short-time decrease at near 12:00.

L360: in Fig. 6c, kappa of larger particles also reaches _0.4 around noon, which is also very close to that of pure AS. But from Fig. 6d we can see there is still a large fraction of hydrophobic and less-hygroscopic species.

Re: As discussed in section 4.2, aerosol particles in this site were highly internal-mixed and aged. κ-PDF for all size particles showed only one hydrophilic mode during daytime although there was still a large fraction of hydrophobic and less-hygroscopic species. This is because the condensation of sulfuric acid on organics or BC can greatly enhance their hygroscopicity (Peng et al., 2016; Zhang et al., 2017).

L370: the growth of the newly formed particles is also driven by condensation of sulfate and organics.

Re: Yes, we have corrected.

L374: why does the PM1 composition differs largely from 40-200 nm particles? 200

nm is in the accumulation mode which is the main contributor of PM1 mass. So I would not expect a large difference between kappa_{chem} and kappa_{gf,200nm}.

Re: The reviewer is right. We have deleted the expression "the bulk chemical compositions of PM_1 and of 40–200 nm particles differ greatly" in the manuscript. The difference was mainly induced by the simple ZSR mixing rule. This feature was stronger at noon when atmospheric oxidation and the aging process were more rapid. We have studied this phenomenon deeply in another paper (Zhang et al., 2017).

L387: Use critical diameter in stead of AR in this section.

Re: As mentioned above, we did not take size-resolved CCN measurement in this campaign, so critical diameter cannot be got directly. We will do the work in the future campaigns.

L394: the number concentration of fine particles. . .

Re: We have corrected.

L400: I do not think one can get this conclusion based on the discussion in this section. The result is in consistent with it but can not directly prove it. Also I think the paper of Dusek et al., (2006) should be cited here. Dusek U, Frank G P, Hildebrandt L, et al. Size matters more than chemistry for cloud-nucleating ability of aerosol particles[J]. Science, 2006, 312(5778):1375.

Re: Figure 11 in this reply depicts the sensibility tests of aerosol size distribution and chemical composition to the CCN number concentration estimation, which are similar with that of Dusek et al., (2006). The figure shows the closure correlation using mean NASD (normalized aerosol size distribution) is weaker than that using mean κ_{chem}, reflecting the more important effect of particle size for aerosol CCN activity than chemical composition. We have added the figure in the supplement and cited this paper in the revised manuscript.

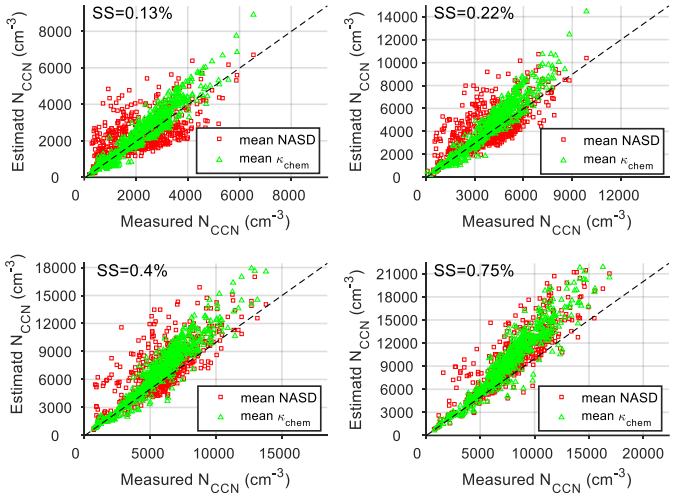

Figure **10**. Correlation between the measured and estimated CCN number concentration. The later was from the mean NASD (normalized aerosol size distribution) but variable composition (κ_{chem}) or using the mean κ_{chem} but variable

NASD.

L407: the critical diameters of aerosol for SS from 0.07% to 0.80% range from about 30 nm to 200 nm. As shown in Fig.6, there is a large difference between kappa_{chem} and kappa_{gf} and the authors claimed that PM1 composition “differ greatly from 40-200 nm particles” (L374). It means one can not use the PM1 composition in the CCN closure. I think a better way might be to compare the kappa obtained from HTDMA and CCN measurements. Although some species may exhibit different kappa in sub- and super-saturation, at least the two measurements are in the same size range.

Re: The related expression “PM_1 composition differ greatly from 40-200 nm particles” is not appropriate, which has been deleted in this manuscript. The κ closure from HTDMA and CCN data is useful to analyze the aerosol hygroscopicity in detail. However, it cannot be realized in this campaign because no size-resolved CCN data. It will be done in the future campaigns.

L434: From this paragraph what I understand is, 0.31 is the average kappa_{chem} and calculated Nccn is not sensitive on the variation of kappa_{chem}. But how can you make sure that 0.31 is a good proxy for the calculation of Nccn in XT? You found some discrepancies between the calculated and measured Nccn and claimed that there are some biases in measured Nccn. So, there is no reference to check which kappa value is appropriate. Normally, water depletion effect can be neglected if Nccn<1e4. Maybe you can try to do the fit for data points <1e4 and >1e4 separately.

Re: Figure 8 in the manuscript shows there is a limited difference for the CCN closure using variable or mean κ_{chem}, so N_{CCN} is not sensitive on the variation of κ_{chem}. 0.31 is only a reference value for people who need to calculate the CCN concentration in this region in their models. As the reviewer says, the CCN closure can be categorized according to N_{CCN}. Actually, the measured N_{CCN} is biased when N_{CCN} > 5500 cm^{-3} (Fig. 12 in this reply), this is coincident with the report from DMT-CCNC manual. Figure 12 in this reply also shows the CCN closure is very good when N_{CCN} < 5500 cm^{-3}, reflecting the validation of the closure method used in this study.

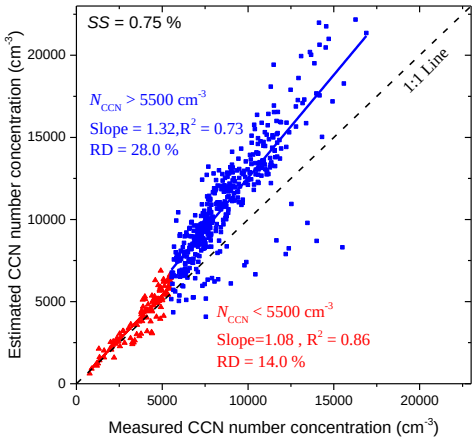

Figure 11. Estimated versus measured CCN number concentrations at SS = 0.75 %. The N_{CCN} is estimated based on κ-Köhler theory, using the real-time κ_{chem}. Here, the critical value of N_{CCN} = 5500 cm^{-3} is used to separate the points into two groups. A separate linear regression analysis is done on each group. The slopes, correlation coefficients (R^2), and relative deviations (RD) are shown in the figure.

L437: the sensitivity of Nccn on aerosol mixing state is not examined in this section.
Re: According to the HTDMA measurement results, aerosols in this region are highly internal-mixed and aged. Therefore, we directly assume aerosols are internally mixed when calculating the CCN number concentration as description in section 3.2.
Another work of our group have suggested the mixing state had a minor effect for the CCN estimation in Beijing (Ren et al., 2017).

References:

Badger C.L., George I., Griffiths P.T., Braban C.F., Cox R.A. and Abbatt J.P.D.: Phase transitions and hygroscopic growth of aerosol particles containing humic acid and mixtures of humic acid and ammonium sulphate, Atmos Chem Phys, 6, 755-768, 10.5194/acp-6-755-2006, 2006.

Dusek U., Frank G.P., Hildebrandt L., Curtius J., Schneider J., Walter S., Chand D., Drewnick F., Hings S. and Jung D.: Size matters more than chemistry for cloud-nucleating ability of aerosol particles., Science, 312, 1375-8, 2006.

Peng J., Hu M., Guo S., Du Z., Zheng J., Shang D., Zamora M.L., Zeng L., Shao M. and Wu Y.: Markedly enhanced absorption and direct radiative forcing of black carbon under polluted urban environments, Proceedings of the National Academy of Sciences, 113, 4266-4271, 2016.

Petters M.D. and Kreidenweis S.M.: A single parameter representation of hygroscopic growth and cloud
condensation nucleus activity, Atmos Chem Phys, 7, 1961-1971, 2007.

Ren J., Zhang F., Wang Y., Fan X., Jin X., Xu W., Sun Y., Cribb M. and Li Z.: Using different assumptions of aerosol mixing state and chemical composition to predict CCN concentrations based

on filed measurement in Beijing, Atmos. Chem. Phys. Discuss., 2017, 1-40, 10.5194/acp-2017-806, 2017.

Rose D., Gunthe S.S., Mikhailov E., Frank G.P., Dusek U., Andreae M.O. and Pöschl U.: Calibration and measurement uncertainties of a continuous-flow cloud condensation nuclei counter (DMT-CCNC): CCN activation of ammonium sulfate and sodium chloride aerosol particles in theory and experiment, Atmos Chem Phys, 8, 1153-1179, 2008.

Tan H., Xu H., Wan Q., Li F., Deng X., Chan P.W., Xia D. and Yin Y.: Design and application of an unattended multifunctional H-TDMA system, J. Atmos Ocean Tech, 30, 1136-1148, 2013.

Wang G., Zhang R., Gomez M.E., Yang L., Zamora M.L., Hu M., Lin Y., Peng J., Guo S. and Meng J.: Persistent sulfate formation from London Fog to Chinese haze, Proceedings of the National Academy of Sciences, 113, 13630-13635, 2016.

Wang Y., Zhao C., Dong Z., Li Z., Hu S., Chen T., Tao F. and Wang Y.: Improved retrieval of cloud base heights from ceilometer using a non-standard instrument method, Atmos Res, 202, 148-155, https://doi.org/10.1016/j.atmosres.2017.11.021, 2018.

Wang Z., Wu Z., Yue D., Shang D., Guo S., Sun J., Ding A., Wang L., Jiang J. and Guo H.: New particle formation in China: Current knowledge and further directions, Sci Total Environ, 577, 258-266, 2017.

Wu Y., Wang X., Tao J., Huang R., Tian P., Cao J., Zhang L., Ho K.F., Han Z. and Zhang R.: Size distribution and source of black carbon aerosol in urban Beijing during winter haze episodes, Atmos Chem Phys, 17, 7965-7975, 10.5194/acp-17-7965-2017, 2017.

Zhang F., Wang Y., Peng J., Ren J., Collins D., Zhang R., Sun Y., Yang X. and Li Z.: Uncertainty in predicting CCN activity of aged and primary aerosols, Journal of Geophysical Research: Atmospheres, 122, 2017.

Zhang Y., Du W., Wang Y., Wang Q., Wang H., Zheng H., Zhang F., Shi H., Bian Y., Han Y., Fu P., Canonaco F., Pre vo^t A.S.H., Zhu T., Wang P., Li Z. and Sun Y.: Aerosol chemistry and particle growth events at an urban downwind site in the North China Plain, Atmos. Chem. Phys. Discuss., 2018, 1-29, 10.5194/acp-2017-889, 2018.

Characterization of aerosol hygroscopicity, mixing state, and CCN activity at a suburban site in the central North China Plain

Yuying Wang[1], Zhanqing Li[1], Yingjie Zhang[2], Wei Du[2,3], Fang Zhang[1] , Haobo Tan[4], Hanbing Xu[5], Tianyi Fan[1], Xiaoai Jin[1], Xinxin Fan[1], Zipeng Dong[1], Qiuyan Wang[6], Yele Sun[2,3]

[1]College of Global Change and Earth System Science, Beijing Normal University, Beijing 100875, China

[2]State Key Laboratory of Atmospheric Boundary Layer Physics and Atmospheric Chemistry, Institute of Atmospheric Physics, Chinese Academy of Sciences, Beijing 100029, China

[3]College of Earth Sciences, University of Chinese Academy of Sciences, Beijing 100049, China

[4]Key Laboratory of Regional Numerical Weather Prediction, Institute of Tropical and Marine Meteorology, China Meteorological Administration, Guangzhou 510080, China

[5]Shared Experimental Education Center, Sun Yat-sen University, Guangzhou 510275, China

[6]Collaborative Innovation Center on Forecast and Evaluation of Meteorological Disasters, Nanjing University of Information Science and Technology, Nanjing, 210044, China

Correspondence to: Zhanqing Li (zli@atmos.umd.edu)

带格式的: 字体: 10.5 磅

带格式的: 字体: (默认) Times New Roman

Abstract. Aerosol hygroscopicity, mixing state and CCN activity were investigated as a part of the Atmosphere-Aerosol-Boundary Layer-Cloud (A^2BC) Interaction Joint Experiment carried out at Xingtai (XT), a suburban site in the center of the North China Plain (NCP). In general, the probability density function of the hygroscopicity parameter (κ-PDF) for 40–200 nm particles had a unimodal distribution and mean κ-PDF patterns for different sizes were similar, suggesting that the particles were highly aged and internally mixed because of strong photochemical reactions. The κ calculated from ~~the~~ hygroscopic growth factor in the daytime and at nighttime showed that photochemical reactions largely enhanced the aerosol hygroscopicity, and the effect became weaker as the particle size increased. In addition, the aerosol hygroscopicity was much larger at XT than at sites in the northern part of the NCP, illustrating that the hygroscopicity of particles varies largely due to different emissions and chemical processes in the NCP.

Measurement results also showed that new particle formation events occurred frequently at XT, one of the most polluted city in China. The evolution of the planetary boundary layer played a dominant role in aerosol mass concentration changes while particle formation and growth had a greater influence on the variation in aerosol number concentrations. Particle size was the most important factor influencing the ability of aerosols to activate, especially at higher levels of supersaturation (SS). The cloud condensation nuclei (CCN) number concentration (N_{CCN}) derived from chemical composition was highly correlated with the measured N_{CCN} ($R^2 \geqslant 0.85$), but was generally overestimated due to measurement uncertainties.

The effect of chemical composition on N_{CCN} was weaker relative to the particle size. N_{CCN} sensitivity tests showed that the impact of chemical composition on N_{CCN} became weaker with increasing SS, suggesting that chemical composition played a less role in N_{CCN} estimationss at higher SS levelss. A good proxy for the chemical comical composition (κ = 0.31) was found, which can simplify the calculation of N_{CCN} on models.

1. Introduction

Aerosols, defined as the mixture of solid and liquid particles suspended in air, are ubiquitously present in the atmosphere because of direct emissions from biogenic and anthropogenic sources and the secondary transformation from gas precursors. Aerosol particles play an important role in climate changes through direct and indirect effects (e.g. Ramanathan et al., 2001; Daniel et al., 2008; Z. Li et al., 2016). However, the impact of aerosols on climate change is difficult to simulate because of the highly variable physical and chemical properties of aerosols, and complex aerosol-cloud interactions (IPCC, 2013; Lebo et al., 2017).

The hygroscopic growth and mixing state of aerosol particles are important for estimating the direct climate effect of aerosols. This is because the growth and mixing can change the particle size and optical properties of aerosol particles, directly influencing the terrestrial radiation budget and degrading the atmospheric visibility (e.g. Covert et al., 1972; Stock et al., 2011; Peng et al., 2016; Z. Li et al., 2017). In addition, aerosol particles can be activated as cloud condensation nuclei (CCN) under

域代码已更改

域代码已更改

域代码已更改

supersaturation (SS) conditions. The variability in CCN number concentration (N_{CCN}) can modify cloud microphysical properties, thereby causing an indirect radiative forcing (Twomey, 1974; Albrecht, 1989). Previous studies have addressed three main aerosol properties influencing the CCN activation, namely, particle size, chemical composition, and mixing state. However, their relative importance is different in different environments (e.g. Dusek et al., 2006; Ervens et al., 2007; Cubison et al., 2008; Deng et al., 2011; Zhang et al., 2014; Schmale et al., 2018).

Ambient aerosols are composed of different species, including inorganic ions, organic components, black carbon (BC), and mineral dust. Inorganics mainly contain sulfate, nitrate, and ammonium, while organic aerosols (OA) consist of thousands of chemicals (Jacobson et al., 2000). The hygroscopicity and CCN activity of a single component can be characterized according to laboratory studies (e.g. Petters and Kreidenweis, 2007), but the properties of their mixtures are hard to estimate because of the different chemical species and mixing states of particles in the atmosphere. Therefore, aerosol hygroscopicity and CCN activity are very different in different regions due to different chemical compositions. Comprehensive field measurements of aerosol properties in different areas are necessary to improve models.

China, especially the North China Plain (NCP), has been suffered from severe air pollution since its rapid industrialization and urbanization in the last couple of decades, where diverse sources and aging processes make aerosol properties particularly diverse and complex. As such, the region has drawn much attention in studying the aerosol mixing state, hygroscopicity, and CCN activity (Deng et al., 2011;

域代码已更改

带格式的: 字体: (默认) Times New Roman, (中文) +中文正文 (等线), 字体颜色: 自定义颜色(RGB(8,0,0)), 英语(美国)

带格式的: 字体: (默认) Times New Roman, (中文) +中文正文 (等线), 字体颜色: 自定义颜色(RGB(8,0,0))

域代码已更改

带格式的: 字体: (默认) Times New Roman, (中文) +中文正文 (等线), 字体颜色: 自定义颜色(RGB(8,0,0)), 英语(美国)

域代码已更改

域代码已更改

域代码已更改

Liu et al., 2011; Zhang et al., 2014; F. Zhang et al., 2016; S.L. Zhang et al., 2016; Wu et al., 2016; Y. Wang et al., 2017). Liu et al. (2011) and Y. Wang et al. (2017) have suggested that ambient particles are mostly an external mixture with different hygroscopicities. Deng et al. (2011) has shown that the aerosol number size distribution is critical in the prediction of N_{CCN} while Zhang et al. (2014, 2017) have highlighted the importance of chemical composition in determining particle activation properties. However, all these studies were done using data from the northern part of the NCP. Few studies have focused on the central region of the NCP. Compared to the northern part of the NCP, the central part of the NCP is more affected by industrial emissions where a dense cluster of China's heavy industries exist (Fu et al., 2014). Measurement of aerosol properties in the central part of the NCP are critically needed to investigate the impact of air pollution on the environment and climate changes.

域代码已更改

域代码已更改

域代码已更改

域代码已更改

Xingtai (XT), a city located in the ~~middle~~ central area of the NCP, often ranks in the top of polluted cities in China. Local industrial and domestic sources are the greatest contributors to severe haze events (Wang et al., 2014). A field experiment called the Atmosphere-Aerosol-Boundary Layer-Cloud (A^2BC) Interaction Joint Experiment was carried out at a suburban site in Xingtai in the summer of 2016. Differences in aerosol properties at this site and at sites in the northern part of the NCP were found in this study.

The paper is organized as follows. Sections 2 and 3 describe the measurement method and data analysis theory. Section 4 presents and discusses the measurement results, which includes the data time series, aerosol mixing state, hygroscopicity, CCN

prediction and its sensitivity to chemical composition. A summary and conclusions are given in section 5.

2. Measurements

2.1. Sampling site and meteorology

The A^2BC was carried out at the National Meteorological Basic Station~~national weather station~~ located in XT (37.18° N, 114.~~36°~~ 37° E, 180 m ASL) from 1 May to 15 June of 2016. This suburban site is situated ~ 17 km northwest of Xingtai urban area in southern Heibei Province, located in the central part of the NCP and to the east of Taihang Mountains (Fig. 1a). This region is heavily populated, urbanized, and industrialized. The major industrial manufacturers include coal-based power plants, steel and iron works, glassworks, and cement mills. The weak diffusion conditions and heavy industrial emissions lead to exceptionally high concentrations of particulate matter (PM) with diameter less than 10 μm (PM_{10}) and 2.5 μm ($PM_{2.5}$), as well as gas pollutants such as sulfur dioxide (SO_2), volatile organic compounds (VOCs) and nitrogen oxides (NO_x) during the frequent occurring haze episodes in this region (Wang et al., 2014; Fu et al., 2014). Figure 1b shows the mean distribution of SO_2 concentrations from May of 2012 to 2016, confirming that the measurement site is located in one of the pollution centers in~~of~~ this region. The detailed analysis of gas precursors and aerosol chemical species shows this station is a good representative site in this region (Zhang et al., 2018).

Time series of meteorological variables measured at ~~the~~ this ~~weather~~

带格式的: 字体: (默认) Times New Roman, (中文) 宋体, 12 磅

域代码已更改

meteorological station are shown in Fig. S1. This site is heavily affected by the mountain-valley wind, showing a prevailing southeasterly wind during the day and a northwesterly wind at night (Fig. S1 and Fig. S2). There was almost no precipitation during the study period. The ambient temperature (T) and relative humidity (RH) time series show opposing trends. Campaign-mean values of T and RH are 21.9 °C and 51.6 %, respectively.

2.2. Instrumentation and operation

2.2.1. Aerosol hygroscopicity measurements

~~The~~ The custom-built hygroscopicity tandem differential mobility analyzer (H-TDMA) used in this study has been described in detail by others (Tan et al., 2013; Y. Wang et al., 2017). Briefly, ambient aerosols are first dried and neutralized by a Nafion dryer and a soft X-ray charger. A differential mobility analyzer (DMA_1, model 3081L, TSI Inc.) is used to select monodispersed particles of a certain diameter (D_{p0}). The monodisperses particles are then pass~~ed~~ through ~~a~~a n~~N~~afion humidifier with a controlled higher RH and are humidified. A second DMA (DMA_2, same model as the DMA_1) and a water-based condensation particle counter (WCPC, model 3787, TSI Inc.) are used to measure the number size distribution of the humidified particles. The DMA_1 and WCPC can also be connected directly to measure the 10–400 nm particle number size distribution (PNSD). In this study, the dry diameters selected by the DMA_1 are 40, 80, 110, 150, and 200 nm. The humidified RH is set to 85 %, the RH calibration with ammonium sulfate for the HTDMA is shown in Fig. S3 in the

域代码已更改

supplement.

The hygroscopic growth factor (GF) is defined as the ratio of the humidified diameter at a given RH to the dry diameter:

$$\mathrm{GF} = \frac{D_{\mathrm{p}}(\mathrm{RH})}{D_{\mathrm{p0}}}, \quad (1)$$

where $D_{\mathrm{p}}(\mathrm{RH})$ is the particle diameter at the given RH and D_{p0} is the dry diameter selected by the DMA_1. The measured distribution function versus GF (GF-MDF) can be calculated with WCPC data downstream from the DMA_1 and DMA_2. The GF probability density function (GF-PDF) is then retrieved using the TDMAFIT algorithm (Stolzenburg and McMurry, 1988, 2008).

2.2.2. Aerosol chemical composition measurements

~~The~~An Aerosol Chemical Speciation Monitor (ACSM) was deployed to measure the non-refractory submicron aerosol ($\mathrm{NR\text{-}PM}_1$) species (sulfate, nitrate, ammonium, chloride, and organics) in real-time. A $\mathrm{PM}_{2.5}$ URG cyclone (model URG-2000-30ED) was installed in the front of the sampling inlet to remove coarse particles (> 2.5 μm in diameter). Before sampling into the ACSM, aerosol particles were dried (below 40 % RH) by a silica gel diffusion dryer. In addition, the ACSM was calibrated routinely with pure ammonium nitrate to determine its ionization efficiency. More detailed descriptions about the ACSM are given by Ng et al., (2011) and Sun et al., (2012). A positive matrix factor analysis is used to analyze the organic spectral matrices according to Ulbrich et al., (2009). Three factors, i.e., hydrocarbon-like OA (HOA), cooking OA (COA), and oxygenated OA (OOA), are chosen as the ACSM dataset.

带格式的: 字体: Times New Roman
带格式的: 行距: 单倍行距
带格式的: 字体: Times New Roman
域代码已更改
域代码已更改
域代码已更改
域代码已更改

HOA and COA are both ~~anthropogenic~~ primary organic aerosols (POA) while OOA is the secondary organic aerosol (SOA).

The ACSM does not detect refractory material such as BC, so a seven-wavelength aethalometer (AE-33, Magee Scientific Corp.) was used to measure the BC mass concentration of BC particles with diameters < 1.0 μm (BC PM_1). Mineral dust and sea salt are the other refractory species, but they typically exist in the coarse mode and make negligible contributions to PM_1 (Juranyi et al., 2010; Meng et al., 2014).

域代码已更改

2.2.3. Aerosol size distribution and CCN measurements

The aerosol particle number size distribution (15–685 nm) was measured by a scanning mobility particle sizer (SMPS) that was equipped with a long DMA (model 3081L, TSI Inc.) and a condensation particle counter (CPC, model 3775, TSI Inc.). A single-column continuous-flow ~~stream-wise~~ thermal-gradient cloud condensation nuclei counter (CCNC-100, DMT Inc.) was applied to measure the bulk CCN number concentration. Five SS levels, i.e., 0.07, 0.1, 0.2, 0.4, and 0.8 %, were set in the CCNC and the running time was 10 min for each SS level. The SS in the CCNC ~~are~~ were calibrated with pure ammonium sulfate (Rose et al., 2008) before and after the measurement campaign. The corrected SS levels ~~are~~ were 0.11, 0.13, 0.22, 0.40, and 0.75 %, respectively.

域代码已更改

The aerosol activation ratio (AR) at a certain SS is calculated as N_{CCN} divided by the total particle number concentration in the 15–685 nm range ($N_{15–685\ nm}$), i.e., AR = N_{CCN} / $N_{15–685\ nm}$. The particle number concentration below 15 nm is not measured by

the SMPS, but this does not affect the calculated N_{CCN} because the activation critical diameter is always larger than 15 nm at these SS levels (Zhang et al., 2014). Aerosol particles with diameters larger than 685 nm are also not detected by the SMPS. These larger particles will always act as CCN due to their larger dry sizes. However, the number concentration above 685 nm in the atmosphere is always negligible (Juranyi et al., 2010).

域代码已更改

域代码已更改

2.2.4. Other measurements

In this study, a micro-pulse lidar (MPL-4B, Sigmaspace Corp.) was used to study the evolution of the planetary boundary layer (PBL). The pulse repetition rate of the MPL wawas 2.5 kHz at a visible wavelength of 532 nm. The peak value of the optical energy of the laser beam was 8 μJ. The pulse duration ranged from 10 to 100 ns, and the pulse interval was set to 200 ns, corresponding to a spatial resolution of 30 m. The MPL-retrieved PBL height is the altitude where a sudden decrease in the scattering coefficient occurs (Brooks, 2003; Quan et al., 2013).

域代码已更改

Trace gas analyzers (manufactured by ECOTECH) were used to measure the gaseous species of ozone (O_3,) and SO_2, NOx, NO and CO. ~~SO_2 was measured using an SO_2 analyzer with a fluorescence cell (Ecotech model 9850A) and O_3 was measured using an O_3 analyzer (Ecotech model 9810B) with ultraviolet absorption technology.~~ More detailed descriptions about the ~~trace gas~~ analyzers are given by Zhu et al., (2016).

带格式的: 字体: (默认) Times New Roman, (中文) +中文正文 (等线), 12 磅

域代码已更改

During this campaign, all sampling instruments were placed in two containers at

ground level and two air conditioners were used to maintain the temperature at 20–25 °C inside containers. All stainless tube inlets were ~ 1.5 m above the top of containers.

3. Theory

3.1. Hygroscopicity parameter

To link hygroscopicity measurements below and above water vapor saturation, the Köhler theory (Köhler, 1936) is parameterized using the hygroscopicity parameter κ (Petters and Kreidenweis, 2007). This is known as the κ-Köhler theory. According to the theory, the equilibrium equation over a solution droplet at a saturation ratio $S(D)$ is

$$S(D) = \frac{D^3 - D_d^3}{D^3 - D_d^3(1-\kappa)} \exp\left(\frac{4\sigma_{s/a} M_w}{RT\rho_w D}\right) , \quad (2)$$

where D and D_d are the wet and dry droplet diameters, respectively, $\sigma_{s/a}$ is the surface tension coefficient, M_w is the mole mass of water, R is the universal gas constant, T is the temperature, and ρ_w is the density of water.

Below the water vapor saturation, $S(D)$ is RH, D is D_p(RH), and D_d is D_{p0} in Eq. (1). The κ parameter is then calculated using H-TDMA data according to Eq. (1) and Eq. (2):

$$\kappa_{gf} = (GF^3 - 1) \cdot \left[\frac{1}{RH} \exp\left(\frac{4\sigma_{s/a} M_w}{RT\rho_w D_d GF}\right) - 1\right] . \quad (3)$$

For a multicomponent particle, the Zdanovskii–Stokes–Robinson (ZSR) mixing rule (Stokes and Robinson, 1966) can also estimate κ using chemical composition data:

$$\kappa_{chem} = \sum_i \varepsilon_i \kappa_i , \quad (4)$$

域代码已更改

域代码已更改

带格式的: 字体: Times New Roman

带格式的: 行距: 单倍行距

带格式的: 字体: Times New Roman

带格式的: 字体: Times New Roman

带格式的: 字体: Times New Roman

带格式的: 行距: 单倍行距

域代码已更改

带格式的: 字体: Times New Roman

带格式的: 行距: 单倍行距

带格式的: 字体: Times New Roman

带格式的: 样式3 字符

where ε_i and κ_i are the volume fraction and hygroscopicity parameter for the ith chemical component. The ACSM provides the mass concentrations of inorganic ions and organics. A simplified ion-pairing scheme such as that described by Gysel et al., (2007) ~~was~~ is applied to convert ion mass concentrations to mass concentrations of their corresponding inorganic salts (see Table S1 in the supplement). Table S1 also lists κ and the gravimetric density of each individual component under supersaturated conditions. In the following discussions, κ_{gf} and κ_{chem} denote the hygroscopicity parameters derived from H-TDMA measurements and estimated using the ZSR mixing rule, respectively.

3.2. CCN estimation

The critical supersaturation (s_c, ~~s_c sc~~ = S_c-1) for a dry diameter (D_d) of a particle with hygroscopicity κ is calculated from the maximum of the κ-Köhler curve (Eq. ~~1~~2) (Petters and Kreidenweis, 2007). The D_d is also the critical diameter corresponding to the s_c when κ is known, so t~~T~~he s_c~~sc~~-D_d~~Dd~~ relationship ~~is then~~can be established. According to this relationship, the critical diameter ($D_{0,\mathrm{crit}}$) can be calculated using the estimated κ_{chem} (Eq. 4) at a given~~the~~ SS ~~set in the CCNC~~. All particles larger than $D_{0,\mathrm{crit}}$ will activate as CCN, assuming that aerosols are internally mixed. Then the CCN number concentration can be estimated from the integral of the aerosol size distribution provided by the SMPS from $D_{0,\mathrm{crit}}$ to the ~~largest~~ maximum measured size (D_{max}) following Eq. (5):

$$N_{\mathrm{CCN}}(\mathrm{SS}) = \int_{D_{0,\mathrm{crit(SS)}}}^{D_{\mathrm{max}}} \frac{dN(D)}{d\log(D)} d\log(D) \quad (5)$$

$N_{\mathrm{CCN}}(\mathrm{SS})$ can then be compared to the number of CCN at the same SS measured by

域代码已更改

带格式的: 字体: (默认) Times New Roman, 12 磅

带格式的 ...

带格式的: 公式, 缩进: 首行缩进: 0 厘米, 行距: 单倍行距

带格式的: 样式3 字符, 字体: Cambria Math

带格式的: 字体: Times New Roman

the CCNC (i.e. a closure study).

4. Results and discussion

4.1. Overview

Figures 2 and 3 show the time series of the main aerosol properties during the field experimentthis campaign. The PNSD changes dramatically (Fig. 2a) and the aerosol number concentration in the 15–50 nm range ($N_{15–50\ nm}$) increases sharply in the morning almost every day (Fig. 2b). The time series of the mean diameter ($D_P D_m$) of particles also shows that a growth process occurs after the sharp increase in $N_{15–50\ nm}$. All these phenomena suggest that new particle formation (NPF) events occurred frequently at XT during the field experiment (Kulmala et al., 2012; Y. Li et al., 2017). This is likely related to the high concentration of gas precursors mainly from local emissions. High emissions of SO_2 and volatile organic compounds (VOCs) associated with the high oxidation capacity in a polluted atmosphere make NPF events occur more frequently in north China (Z. Wang et al., 2017).

Figure 2c-d shows the time series of the probability density function of κ_{gf} (κ-PDF) for 40 nm and 150 nm particles, respectively. In general, mono-modal κ-PDFs are were observed. This is different from κ-PDFs at other sites in China where bi- and tri-modal distributions are dominant (Liu et al., 2011; Ye et al., 2013; Jiang et al., 2016; S.L. Zhang et al., 2016; Y. Wang et al., 2017). This is due to differences in the aerosol mixing state, which will be discussed in section 4.2.

带格式的: 字体: (中文) +中文正文 (等线)

域代码已更改

域代码已更改

域代码已更改

The bulk mass concentrations of organics, sulfate, nitrate, ammonium, and chloride measured by the ACSM are shown in Fig. 3a, along with the BC mass concentration measured with the AE-33. Organics and sulfate ~~are~~ were the dominant chemical species with mass fractions in PM_1 of 39.1 % and 24.7 %, respectively. Figure 3b-c shows the volume fractions of paired chemical compositions and the hygroscopicity parameter— (κ_{chem}) derived from chemical compositions~~κ_{chem}~~, respectively. The average volume fraction of inorganics ($(NH_4)_2SO_4$+NH_4HSO_4+H_2SO_4+NH_4NO_4) ~~is~~ was similar to that of organics (POA+SOA), but their volume fractions changed diurnally. In general, t~~T~~he volume fraction of inorganics ~~increases~~ increased during daytime while the volume fraction of organics ~~decreases~~decreased. In addition, SOA ~~is~~ was the dominant contributor to OA, accounting for ~69 % of the organics volume. This shows that photochemical reactions were strong at XT during this campaign~~the field experiment~~ (Huang et al., 2014). The mean κ_{chem} in Fig. 3c ~~is~~ was 0.31 with values ranging from 0.20 to 0.40. The trend in κ_{chem} ~~is~~ was similar to that of the volume fraction of inorganics, suggesting that inorganics ~~played~~ plays a key role when it ~~comes~~ comes ~~to~~to –κ_{chem}. this is consistent with the study of (Wu et al., (2016).

域代码已更改

域代码已更改

4.2. Aerosol mixing state and hygroscopicity

The average probability density functions of κ_{gf} (κ-PDF) for different particle sizes derived from H-TDMA data are shown in Fig. 4. For all particle sizes considered, κ_{gf} ~~ranges~~ ranged from 0 to 0.8 and the κ-PDF patterns ~~are~~ were similar, suggesting

751 that the hygroscopic compounds in different particle size mode were~~were~~ similar at
752 XT~~ during the field experiment~~. In general, κ-PDF patterns show only one
753 hydrophilic mode with the weak hydrophobic mode~~s~~ occasionally appearing at night
754 when photochemical reactions are weak (Fig. ~~S3~~S4). This is different from what has
755 been reported at other sites in China (Liu et al., 2011; Ye et al., 2013; Jiang et al.,
756 2016; Zhang et al., 2016; Y. Wang et al., 2017) where the κ-PDF patterns always
757 show bi- or tri-modal distributions. Based on previous studies (Liu et al., 2011; Y.
758 Wang et al., 2017), ambient aerosols can be classified into three groups according to
759 their κ_{gf} values:

760 — nearly hydrophobic (NH): $\kappa_{gf} < 0.1$

761 — less hygroscopic (LH): $0.1 \leqslant \kappa_{gf} < 0.2$

762 — more hygroscopic (MH): $0.2 \leqslant \kappa_{gf}$

763 Table 1 gives the number fractions of each group for different particle sizes. The MH
764 group ~~dominates~~ dominated all particle sizes. The number fractions of the NH and LH
765 groups ~~are~~ were less than 6.0 % each. However, the volume fractions of hydrophobic
766 BC and low-hygroscopic organics (where κ_{BC} is approximately zero and $\kappa_{organic}$ is
767 typically less than 0.1) ~~are~~ were ~10.1 % and 47.4 % according to chemical
768 composition measurements (Fig. 3b). This suggests that the particles were highly aged
769 and internally mixed at XT during th~~e field experiment~~is campaign. Coating of
770 sulfates and secondary organics during the aging process changes the structure of BC
771 and makes it grow, which can significantly enhance the hygroscopicity of particles
772 (e.g., Zhang et al., 2008; Jimenez et al., 2009; Tritscher et al., 2011; Guo et al., 2016).

带格式的: 字体颜色: 红色
带格式的: 字体颜色: 自动设置
域代码已更改
域代码已更改
域代码已更改

In addition, the observed unimodal distribution of κ-PDF also suggests the ~~highly~~ ~~internal~~internal~~ly~~ mix~~ing~~ed~~ state of the particles (Swietlicki et al., 2008).

Figure 5 shows the average size-resolved κ_{gf} derived from H-TDMA data at XT and at other sites in China. At XT, κ_{gf} for different particle sizes ~~are~~ were larger in the daytime than at night and the difference between daytime and nighttime ~~decreases~~ decreased with increasing particle size. This suggests that the impact of photochemical reactions on aerosol hygroscopicity ~~i~~~~was~~ strong and that the effect ~~i~~~~was~~ weaker with increasing particle size because most of the larger particles are always well aged.

The magnitude of κ_{gf} ~~is~~ was larger at XT than at other sites of China. In particular, the magnitude of κ_{gf} wa ~~i~~s much larger at XT than at sites in the northern part of the NCP, i.e., Beijing, Wuqing, and Xianghe. The lower κ_{gf} in the urban area of Beijing is likely related to the more severe traffic emissions (Ye et al., 2013; Wu et al., 2016). Wuqing and Xianghe are located in the suburban area between the two megacities of Beijing and Tianjin and are simultaneously affected by traffic and industrial emissions. The magnitude of κ_{gf} at these two sites are higher than at Beijing but lower than at XT. Although XT is located far away from these megacities, it is situated in the industrial center of the NCP, so the higher concentrations of precursors and strong photo chemical reactions make the particles more internally mixed and highly aged. This is why κ_{gf} in XT is larger than at other sites. This suggests that the hygroscopicity of particles from different emissions and chemical processes differ in NCP. In addition, 40 nm particles ~~are~~ were always more

域代码已更改

带格式的: 字体: (默认) Times New Roman, (中文) 宋体, 12 磅

带格式的: 字体: (默认) Times New Roman, (中文) 宋体, 12 磅

域代码已更改

hygroscopic than 80 nm particles at XT, especially in the daytime, which ~~is~~ was also different from other sites. This is likely because the coating effect of sulfates and secondary organics is more significant on smaller particles (Tritscher et al., 2011; Guo et al., 2016). Furthermore, since the field measurements took place in a local with heavy industrial activities, it is possible that amine contributes significantly to the hygroscopicity of 40 nm particles. Several studies have shown that amine compounds in aerosol phase can be hygroscopic, sometimes at even low RH (e.g. Qiu and Zhang, 2012; Chu et al., 2015; Gomez-Hernandez et al., 2016). ~~.~~

4.3. Diurnal variations in aerosol properties

4.3.1. Diurnal variations in aerosol number and mass concentrations

Figure 6a shows the diurnal variation in MPL-derived PBL height. PBL height can be determined at the altitude where a sudden decrease in the scattering coefficient occurs from the MPL data (Cohn and Angevine, 2000; Brooks, 2003). Note that the retrieved PBL height is only valid from 07:00 local time (LT) to 19:00 LT (Quan et al., 2013). The retrieved PBL height at night is not accurate because of the likely influence of residual aerosols within the nocturnal PBL. The evolution of PBL height from 07:00 LT to 19:00 LT is sufficient to analyze its link with the change in aerosol number and mass concentrations during the daytime. Figure 6b shows diurnal variations in aerosol number and mass concentrations in the 15–685 nm range ($N_{15–685\ nm}$ and $PM_{15–685\ nm}$, respectively). Variations in the $N_{15–685\ nm}$ and $PM_{15–685\ nm}$ trend~~s~~ed oppose each other. From 08:00 LT to 14:00 LT, the PBL height ~~lifts~~ lifted from ~0.5

域代码已更改

域代码已更改

km to ~0.6 km, while $PM_{15–685\ nm}$ decreaseds from ~24 μg m^{-3} to ~19 μg m^{-3} although there wais a slight increase at the beginning of the period. This suggests the important effect of PBL evolution on $PM_{15–685\ nm}$. However, $N_{15–685\ nm}$ sharply increaseds from ~7600 cm^{-3} at 07:00 LT to ~13000 cm^{-3} at 13:00 LT. This is related to the sudden burst of nucleationsmall Aitken mode particles (< 100 50 nm) when NPF events occurred. Newly formed fine particles contribute little to $PM_{15–685\ nm}$. In the evening, $PM_{15–685\ nm}$ increaseds gradually while $N_{15–685\ nm}$ decreasesdecreased. This is attributed to the declining trend in the nocturnal PBL and particle coagulation and growth. In other words, the evolution of the PBL plays played a dominant role on the aerosol mass concentration, while particle formation and growth has had a greater influence on the variation in aerosol number concentration.

4.3.2. Diurnal variation in aerosol hygroscopicity

Figure 6c shows diurnal variations in κ_{gf} and κ_{chem}. All sized κ_{gf} increases increased beginning from the NPF event, especially for the 40 nm particles. The increase of κ_{gf} in the morning wawas synchronous with the particle number concentration ($N_{15–685\ nm}$) but not with the PBL height, further suggesting the impact of photochemical reactions on aerosol hygroscopicity. The κ_{gf} for 40 nm particles increases increased from ~0.32 at 07:00 LT to ~0.44 at 15:00 LT, and approaches approached the κ of pure ammonium sulfate, also [$\kappa_{gf,(NH_4)_2SO_4}$ = 0.48 (Wu et al., 2016)]. This suggestings that a large amount of hygroscopic compoundssulfates were produced through the photochemical reactions of precursorsduring NPF events. Fig.

域代码已更改

S5 in the supplement shows ~~This can be verified from the diurnal variation in~~ the sharply increased concentrations of SO_2 and VOCs in the morning and the enhanced atmospheric oxidation capacity under high RH and low *T* made plenty of sulfate and SOA produced. This is the reason in the increase of aerosol hygroscopicity and the frequent occurrence of NPF events~~chemical composition (Fig. 6d), which shows that the mass fraction of sulfate increased~~. Detailed characterization of aerosol chemistry during NPF events in this campaign has been studied in Zhang et al. (2018). T~~ during the daytime while the mass fraction of organics (POA or SOA) varied more weakly. The diurnal variation in SO_2 precursor also shows this (Fig. S4). T~~he diurnal variation pattern in κ_{gf} for 80–200 nm particles ~~–~~differ~~s~~ from that of 40 nm particles. The differences in κ_{gf} between 80–200 nm particles in the early morning ~~are~~ were large but gradually decrease as the sun rises. After 11:00 LT, the κ_{gf} for 80–200 nm particles ~~are~~ were similar but lower than that of 40 nm particles. All these~~,~~ suggest~~sing that~~ the enhanced hygroscopicity in the ~~80~~40–200 nm particles wa~~s~~was likely~~likely~~ caused by the condensation of sulfates and secondary organics (Fig. 6d) ~~while~~ and the effect was more significant for 40 nm particles~~that of the 40 nm particles was caused by the growth of the new particles~~.

Figure 6c also shows that the κ_{chem} for PM_1 ~~is~~ was lower than the κ_{gf} for 40–200 nm particles and ~~has~~ had a weaker diurnal variation. This feature was stronger at noon when atmospheric oxidation and the aging process were more rapid. ~~Two reasons may explain this: (1) the bulk chemical compositions of PM1 and of 40–200 nm particles differ greatly and (2)~~ The difference was mainly induced by the simple

带格式的: 非上标/ 下标

带格式的: 字体: (默认) Times New Roman, (中文) 宋体, 12 磅, 字体颜色: 自动设置

带格式的: 字体: (默认) Times New Roman, (中文) 宋体, 12 磅, 字体颜色: 自动设置

ZSR mixing rule. ~~the ZSR model cannot describe the impact of condensation on aerosol hygroscopicity very well.~~ During the daytime, the condensation of sulfuric acid on organics or BC greatly enhances their hygroscopicity (Zhang et al., 2008; Zhang et al., ~~2009~~2017). This phenomenon can't be described accurately by the ZSR model. Cruz and Pandis (2000) have shown that the measured κ_{gf} of internally mixed $(NH_4)_2SO_4$-organic aerosols is larger than the predicted κ_{chem} based on the ZSR model.

In summary, the ample supply of effluent SO_2 and VOCs provide~~d~~d sufficient precursors for the strong photochemical reactions at XT during this campaign~~e field experiment~~, and the produce~~ and d sulfates and the~~ condensation of sulfate and SOA~~uric acid~~ enhance~~d~~d aerosol hygroscopicity largely, especially during the daytime. This also suggests that the observed frequent NPF events ~~were~~ were mainly induced by the oxidation of precursors.

4.3.3. Diurnal variation in CCN number concentration and activation ratio

Figure 7a shows the diurnal variations in N_{CCN} and AR at different SS. In the morning, N_{CCN} first ~~decreases~~ decreased then ~~increases~~ increased while AR ~~shows~~ showed the opposite trend. This is related to the evolution of the PBL and NPF events. At the initial stage of an NPF event, the newly formed particles ~~are~~ were less than 15 nm in size, which ~~is~~ was below the detection limit of the SMPS. As a result, $N_{15-685\,nm}$ ~~decreases~~ decreased (Fig. 6b) as the PBL lifts and N_{CCN} also ~~decreases~~decreased. However, the mixing of aged particles within the PBL made~~s~~ the particle size (Fig.

域代码已更改

带格式的: 字体: (默认) Times New Roman, (中文) 宋体, 12 磅, 字体颜色: 自动设置

域代码已更改

7b) and AR increase slightly. With condensation and the growth of new particles, the number of fine particles detected by the SMPS increased rapidly but a portion of them cannot be activated because their smaller size. Therefore, ~~So~~ N_{CCN} ~~increases~~ increased but AR ~~decreases~~ decreased from 08:00 LT to 14:00 LT. In the afternoon and evening, N_{CCN} and AR increased slightly with the increase in particle size (Fig. 7b). However, these trends ~~become~~ became weaker as SS ~~decreases~~decreased, this is~~likely~~ because the critical diameter is larger at low SS and the influence of aerosol size distribution on N_{CCN} and AR is relatively weaker. This demonstrates that the particle size ~~is~~ was the most important factor influencing the aerosol activation ability and the CCN number concentration, especially at larger SS levels. The sensitivity test of particle size in CCN closure study similar with that in Dusek et al. (2006) was shown in Fig. S6.

带格式的: 字体: 倾斜

带格式的: 字体: 倾斜

带格式的: 字体: (默认) Times New Roman, (中文) 宋体, 字体颜色: 自动设置, 英语(美国)

带格式的: 字体: (默认) Times New Roman, (中文) 宋体, 字体颜色: 自动设置, 英语(美国)

带格式的: 字体: (默认) Times New Roman, (中文) 宋体, 字体颜色: 自动设置, 英语(美国)

4.4. CCN estimation from chemical composition data

The three main factors influencing CCN activation are particle size, mixing state, and chemical composition. As discussed in the above sections, particles ~~are~~ were highly internally mixed at XT and particle size ~~has~~ had a great influence on N_{CCN}. In this section, a CCN closure study ~~is~~ is conducted and the impact of chemical composition on N_{CCN} is discussed. Figure 8a shows estimated N_{CCN} as a function of measured N_{CCN} using real-time κ_{chem}. The estimated N_{CCN} correlates well with measurements ($R^2 \geqslant 0.85$) but is generally overestimated. The slope of each linearly fitted line is greater than 1.10 and increases with increasing SS. In addition, the

relative deviation (RD) increases from 16.2 % to 25.2 % as SS increases from 0.13 % to 0.75 %, suggesting that estimates become worse at larger SS. The overestimation of N_{CCN} is mainly caused by large measurement uncertainties of CCNC: (1) the temperature or high flow rates in the CCNC may not allow enough time for particles to reach sizes large enough to be counted by the OPC at the exit of the CCN chamber (Lance et al., 2006; Cubison et al., 2008) and (2) in high particle number concentration environments, water depletion in the CCNC may reduce the counting rate of the CCNC (Deng et al., 2011). These uncertainties make measured N_{CCN} lower than the actual N_{CCN}. At larger SS, those activated aerosols in the cloud chamber of CCNC are greater in number and smaller in size, so the impact of these uncertainties is greater. The separated N_{CCN} closure study is shown in ~~Another discussion about this problem can be found in the supplement (~~Fig. ~~S5~~S7~~)~~. Figure S7 suggests the CCN closure is very good when N_{CCN} < 5500 cm^{-3}, reflecting the validation of the CCN closure method in this study.

Figure 8b shows estimated N_{CCN} using the mean value for κ_{chem} (κ_{chem} = 0.31). Compared with results using real-time values for κ_{chem}, the fit parameters and RD change slightly, suggesting that the effect of chemical composition on N_{CCN} is weaker relative to the particle size. The sensitivity of estimated N_{CCN} to the variability in chemical composition (κ_{chem}) is further investigated (Fig. 9). In this figure, the variability of the equipotential lines in RD suggests that the sensitivity of N_{CCN} is strongly time dependent. This is attributed to the variability of the shape of the aerosol size distribution (Juranyi et al., 2010), further verifying the importance of particle size

域代码已更改

带格式的: 字体: 倾斜

域代码已更改

带格式的: 字体: 倾斜

带格式的: 字体颜色: 文字 1

带格式的: 字体: (默认) Times New Roman, (中文) 宋体, 12 磅, 字体颜色: 文字 1

带格式的: 字体: 倾斜

域代码已更改

to N_{CCN}. The sensitivity of N_{CCN} to chemical composition (κ_{chem}) becomes weaker with increasing SS, suggesting that chemical composition becomes less important in N_{CCN} estimates at larger SS. In addition, the RD is always less than 10 % when estimating N_{CCN} using the mean value of κ_{chem}, suggesting that κ = 0.31 is a good proxy for chemical composition when estimating N_{CCN} at XT.

In summary, particle size is the most important factor influencing the aerosol activation ability at XT, especially at larger SS levels. The mixing state and chemical composition were not as important when estimating N_{CCN} because the particles were highly aged and internally mixed at XT ~~during the field experiment~~, and aerosol hygroscopicity was not sensitive to estimates of N_{CCN}.

5. Summary and conclusions

The Atmosphere-Aerosol-Boundary Layer-Cloud (A^2BC) Interaction Joint Experiment was carried out at a ~~polluted~~ suburban site located in the central North China Plain (NCP) from 1 May to 15 June of 2016. The aerosol hygroscopicity, mixing state and CCN activity at the site Xingtai (XT) ~~were~~ were investigated in this study.

In general, the probability density function of the hygroscopicity parameter (κ-PDF) for 40–200 nm particles ~~is~~ was a unimodal distribution, which is different from distributions at other sites in China. Particles of all sizes covered a large range of κ_{gf} (mostly from 0 to 0.8) and showed similar κ-PDF patterns, suggesting that the hygroscopic compounds in these particles from 40 nm to 200 nm were similar at XT.

The κ-PDF patterns also suggests that the particles were highly aged and internally mixed at XT during the ~~field experiment~~this campaign. This is likely related to strong photochemical reactions.

The mean κ_{gf} for different particle sizes ~~are~~ were larger in the daytime than at night. Daytime and nighttime κ_{gf} differences decreased with increasing particle size. This illustrates that the impact of photochemical reactions on aerosol hygroscopicity wa~~s~~as strong and that the effect ~~became~~ became weaker as particle sizes ~~increased~~increases. The enhanced hygroscopicity of 40–200 nm particles ~~was~~ was likely caused by the coating of sulfates or secondary organics ~~while~~ and the effect ~~was~~ was more significant for~~–~~ 40 nm particles. Compared with other sites in China, the aerosol hygroscopicity ~~was~~ was much larger at XT because of ~~the strong photochemical reactions and~~ the sufficient precursors and strong atmospheric oxidation capacity. The comparison also shows that the hygroscopicity of particles from different emissions and chemical processes differed largely.

New particle formation events occurred frequently at XT during ~~the field experiment~~this campaign. The evolution of the planetary boundary layer (PBL) ~~played~~ played a dominant role on the aerosol mass concentration, while particle formation and growth ~~had~~ had a greater influence on the variation in the aerosol number concentration. Particle size ~~was~~ was the most important factor influencing the aerosol activation ability and the CCN number concentration at XT during the field experiment, especially at larger supersaturations (SS). Although the estimated N_{CCN} ~~correlated~~ correlates well with measurements ($R^2 \geqslant 0.85$), N_{CCN} ~~was~~ is

overestimated because of measurement uncertainties. The effect of chemical composition on N_{CCN} ~~was~~ is weaker relative to the particle size. Sensitivity tests show that the impact of chemical composition on N_{CCN} ~~became~~ becomes weaker as SS ~~increased~~increases, suggesting that the effect of chemical composition on N_{CCN} estimates is less important at larger SS. The value κ = 0.31 is a good proxy for chemical composition when estimating N_{CCN} for the model at XT.

Our results show that aerosol properties in the middle of the NCP differ from those in the northern part of the NCP and other regions in China. This is because there are more industrial emissions in the central NCP. The plenitude of gas precursors and strong photochemical reactions at XT make aerosol properties there different from those at sites under other polluted conditions. More field measurements on gas-particle transformation and aerosol properties in this region are needed, which would be meaningful for studying the haze formation mechanism and climate change in the NCP.

Data availability. The data used in the study are available from the first author upon request (wang.yuying@mail.bnu.edu.cn).

带格式的: 字体: (默认) Times New Roman

Competing interests. The authors declare that they have no conflict of interest.

Author contribution. Z.L. and Y.W. designed the experiment, Y.W., Y.Z., and W.D. carried it out and analyzed the data, other co-authors participated in science discussions and suggested analyses. Y.W. prepared the manuscript with contributions from all co-authors.

Acknowledgements. This work was funded by the National Natural Science Foundation of China (NSFC) research projects (grant no. 91544217, 41675141, 41705125), the National Basic Research Program of China "973" (grant no. 2013CB955801), and the China Scholarship Council (award no. 201706040194). We also thank all participants in the field campaign for their tireless work and

cooperation.

域代码已更改

References

Albrecht B.A.: Aerosols, Cloud Microphysics, and Fractional Cloudiness, Science, 245, 1227-30, 1989.

Brooks I.M.: Finding boundary layer top: Application of a wavelet covariance transform to lidar backscatter profiles, J. Atmos. Ocean. Tech., 20, 1092-1105, 2003.

Chu Y., Sauerwein M. and Chan C.K.: Hygroscopic and phase transition properties of alkyl aminium sulfates at low relative humidities, Phys. Chem. Chem. Phys., 17, 19789-19796, https://doi.org/10.1039/c5cp02404h, 2015.

Cohn S.A. and Angevine W.M.: Boundary layer height and entrainment zone thickness measured by lidars and wind-profiling radars, Journal of Applied Meteorology, 39, 1233-1247, 2000.

Covert D.S., Charlson R.J. and Ahlquist N.C.: A study of the relationship of chemical composition and humidity to light scattering by aerosols, Journal of Applied Meteorology, 11, 968-976, 1972.

Cruz C.N. and Pandis S.N.: Deliquescence and hygroscopic growth of mixed inorganic–organic atmospheric aerosol, Environ. Sci. Technol., 34, 4313-4319, https://doi.org/10.1021/es9907109, 2000.

Cubison M.J., Ervens B., Feingold G., Docherty K.S., Ulbrich I.M., Shields L., Prather K., Hering S. and Jimenez J.L.: The influence of chemical composition and mixing state of Los Angeles urban aerosol on CCN number and cloud properties, Atmos. Chem. Phys., 8, 5649-5667, https://doi.org/10.5194/acp-8-5649-2008, 2008.

Daniel R., Ulrike L., Raga G.B., O'Dowd C.D., Markku K., Sandro F., Anni R. and Andreae M.O.: Flood or drought: how do aerosols affect precipitation?, Science, 321, 1309-1313, https://doi.org/10.1126/science.1160606, 2008.

Deng Z.Z., Ma N., Liu P.F., Xu W.Y., Zhao C.S., Ran L., Chen J., Liang Z., Liang S. and Huang M.Y.: Size-resolved and bulk activation properties of aerosols in the North China Plain, Atmos. Chem. Phys., 11, 3835-3846, https://doi.org/10.5194/acp-11-3835-2011, 2011.

Dusek U., Frank G.P., Hildebrandt L., Curtius J., Schneider J., Walter S., Chand D., Drewnick F., Hings S. and Jung D.: Size matters more than chemistry for cloud-nucleating ability of aerosol particles, Science, 312, 1375-1378, https://doi.org/10.1126/science.1125261, 2006.

Eichler H., Cheng Y.F., Birmili W., Nowak A., Wiedensohler A., Brüggemann E., Gnauk T., Herrmann H., Althausen D. and Ansmann A.: Hygroscopic properties and extinction of aerosol particles at ambient relative humidity in South-Eastern China, Atmos Environ, 42, 6321-6334, https://doi.org/10.1016/j.atmosenv.2008.05.007, 2008.

Ervens B., Cubison M., Andrews E., Feingold G., Ogren J.A., Jimenez J.L., DeCarlo P. and Nenes A.: Prediction of cloud condensation nucleus number concentration using measurements of aerosol size distributions and composition and light scattering enhancement due to humidity, J. Geophys. Res.-Atmos., 112, https://doi.org/10.1029/2006JD007426, 2007.

Fu G.Q., Xu W.Y., Yang R.F., Li J.B. and Zhao C.S.: The distribution and trends of fog and haze in the North China Plain over the past 30 years, Atmos. Chem. Phys., 14, 11949-11958, https://doi.org/10.5194/acp-14-11949-2014, 2014.

Gomez-Hernandez M., McKeown M., Secrest J., Marrero-Ortiz W., Lavi A., Rudich Y., Collins D.R. and Zhang R.: Hygroscopic Characteristics of Alkylaminium Carboxylate Aerosols, Environ. Sci. Technol., 50, 2292-2300, https://dx.doi.org/10.1021/acs.est.5b04691, 2016.

Guo S., Hu M., Lin Y., Gomez-Hernandez M., Zamora M.L., Peng J., Collins D.R. and Zhang R.:

带格式的: 字体: (默认) Times New Roman, (中文) +中文正文 (等线), 10 磅, 英语(美国)

带格式的: 字体: (默认) Times New Roman, (中文) +中文正文 (等线), 10 磅, 英语(美国)

带格式的: 字体: (默认) Times New Roman, (中文) +中文正文 (等线), 10 磅, 英语(美国)

带格式的: 字体: (默认) Times New Roman, 10 磅, 字体颜色: 黑色

带格式的: 字体: (默认) Times New Roman, (中文) +中文正文 (等线), 10 磅, 英语(美国)

带格式的: 字体: (默认) Times New Roman

OH-Initiated Oxidation of m-Xylene on Black Carbon Aging, Environ. Sci. Technol., 50, 8605-8612, https://dx.doi.org/10.1021/acs.est.6b01272, 2016.

Gysel M., Crosier J., Topping D.O., Whitehead J.D., Bower K.N., Cubison M.J., Williams P.I., Flynn M.J., McFiggans G.B. and Coe H.: Closure study between chemical composition and hygroscopic growth of aerosol particles during TORCH2, Atmos. Chem. Phys., 7, 6131-6144, https://doi.org/10.5194/acp-7-6131-2007, 2007.

Huang R., Zhang Y., Bozzetti C., Ho K., Cao J., Han Y., Daellenbach K.R., Slowik J.G., Platt S.M., Canonaco F., Zotter P., Wolf R., Pieber S.M., Bruns E.A., Crippa M., Ciarelli G., Piazzalunga A., Schwikowski M., Abbaszade G., Schnelle-Kreis J., Zimmermann R., An Z., Szidat S., Baltensperger U., Haddad I.E. and Prévôt A.S.H.: High secondary aerosol contribution to particulate pollution during haze events in China, Nature, https://doi.org/10.1038/nature13774, 2014.

IPCC: Climate change 2013: Scientific basis, Fifth assessment of the Inter-governmental Panel on Climate Change, Cambridge University Press, 2013.

Jacobson M.C., Hansson H.C., Noone K.J. and Charlson R.J.: Organic atmospheric aerosols: Review and state of the science, Rev. Geophys., 38, 267-294, https://doi.org/10.1029/1998RG000045, 2000.

Jiang R.X., Tan H.B., Tang L.L., Cai M.F., Yin Y., Li F., Liu L., Xu H.B., Chan P.W., Deng X.J. and Wu D.: Comparison of aerosol hygroscopicity and mixing state between winter and summer seasons in Pearl River Delta region, China, Atmos. Res., 169, 160-170, https://doi.org/10.1016/j.atmosres.2015.09.031, 2016.

Jimenez J.L., Canagaratna M.R., Donahue N.M., Prevot A., Zhang Q., Kroll J.H., DeCarlo P.F., Allan J.D., Coe H. and Ng N.L.: Evolution of organic aerosols in the atmosphere, Science, 326, 1525-1529, https://doi.org/10.1126/science.1180353, 2009.

Juranyi Z., Gysel M., Weingartner E., DeCarlo P.F., Kammermann L. and Baltensperger U.: Measured and modelled cloud condensation nuclei number concentration at the high alpine site Jungfraujoch, Atmos. Chem. Phys., 10, 7891-7906, https://doi.org/10.5194/acp-10-7891-2010, 2010.

Köhler H.: The nucleus in and the growth of hygroscopic droplets, Transactions of the Faraday Society, 32, 1152-1161, 1936.

Kulmala M., Petäjä T., Nieminen T., Sipilä M., Manninen H.E., Lehtipalo K., Dal Maso M., Aalto P.P., Junninen H. and Paasonen P.: Measurement of the nucleation of atmospheric aerosol particles, Nat. Protoc., 7, 1651-1667, https://doi.org/10.1038/nprot.2012.091,2012.

Lance S., Nenes A., Medina J. and Smith J.N.: Mapping the operation of the DMT continuous flow CCN counter, Aerosol Sci. Tech., 40, 242-254, http://dx.doi.org/10.1080/02786820500543290, 2006.

Lebo Z.J., Shipway B.J., Fan J., Geresdi I., Hill A., Miltenberger A., Morrison H., Rosenberg P., Varble A. and Xue L.: Challenges for cloud modeling in the context of aerosol-cloud-precipitation interactions, B. Am. Meteorol. Soc., https://doi.org/10.1175/BAMS-D-16-0291.1, 2017.

Li Y., Zhang F., Li Z., Sun L., Wang Z., Li P., Sun Y., Ren J., Wang Y. and Cribb M.: Influences of aerosol physiochemical properties and new particle formation on CCN activity from observation at a suburban site of China, Atmos. Res., 188, 80-89, https://doi.org/10.1016/j.atmosres.2017.01.009, 2017.

Li Z., Lau W.M., Ramanathan V., Wu G., Ding Y., Manoj M.G., Liu J., Qian Y., Li J. and Zhou T.: Aerosol and monsoon climate interactions over Asia, Rev. Geophys., https://doi.org/10.1002/2015RG000500, 2016.

Li Z., Daniel R. and Fan J.W.: Aerosols and Their Impact on Radiation, Clouds, Precipitation, and

带格式的: 字体: (默认) Times New Roman

带格式的: 字体: (默认) Times New Roman

带格式的: 字体: (默认) Times New Roman

Severe Weather Events, Oxford Research Encyclopedias: Environmental science, https://doi.org/10.1093/acrefore/9780199389414.013.126, 2017.

Liu P.F., Zhao C.S., Bel T.G., Hallbauer E., Nowak A., Ran L., Xu W.Y., Deng Z.Z., Ma N., Mildenberger K., Henning S., Stratmann F. and Wiedensohler A.: Hygroscopic properties of aerosol particles at high relative humidity and their diurnal variations in the North China Plain, Atmos. Chem. Phys., https://doi.org/10.5194/acp-11-3479-2011, 2011.

Lopez-Yglesias X.F., Yeung M.C., Dey S.E., Brechtel F.J. and Chan C.K.: Performance Evaluation of the Brechtel Mfg. Humidified Tandem Differential Mobility Analyzer (BMI HTDMA) for Studying Hygroscopic Properties of Aerosol Particles, Aerosol Sci Tech, 48, 969-980, http://dx.doi.org/10.1080/02786826.2014.952366, 2014.

Meng J.W., Yeung M.C., Li Y.J., Lee B.Y.L. and Chan C.K.: Size-resolved cloud condensation nuclei (CCN) activity and closure analysis at the HKUST Supersite in Hong Kong, Atmos. Chem. Phys., 14, 10267-10282, https://doi.org/10.5194/acp-14-10267-2014, 2014.

Ng N.L., Herndon S.C., Trimborn A., Canagaratna M.R., Croteau P.L., Onasch T.B., Sueper D., Worsnop D.R., Zhang Q. and Sun Y.L.: An Aerosol Chemical Speciation Monitor (ACSM) for routine monitoring of the composition and mass concentrations of ambient aerosol, Aerosol Sci. Tech., 45, 780-794, http://dx.doi.org/10.1080/02786826.2011.560211, 2011.

Peng J., Hu M., Guo S., Du Z., Zheng J., Shang D., Zamora M.L., Zeng L., Shao M. and Wu Y.: Markedly enhanced absorption and direct radiative forcing of black carbon under polluted urban environments, Proceedings of the National Academy of Sciences, 113, 4266-4271, https://doi.org/10.1073/pnas.1602310113, 2016.

Petters M.D. and Kreidenweis S.M.: A single parameter representation of hygroscopic growth and cloud condensation nucleus activity, Atmos. Chem. Phys., 7, 1961-1971, https://doi.org/10.5194/acp-7-1961-2007, 2007.

Qiu C. and Zhang R.: Physiochemical Properties of Alkylaminium Sulfates: Hygroscopicity, Thermostability, and Density, Environ. Sci. Technol., 46, 4474-4480, https://dx.doi.org/10.1021/es3004377, 2012.

Quan J., Gao Y., Zhang Q., Tie X., Cao J., Han S., Meng J., Chen P. and Zhao D.: Evolution of planetary boundary layer under different weather conditions, and its impact on aerosol concentrations, Particuology, 11, 34-40, https://doi.org/10.1016/j.partic.2012.04.005, 2013.

Ramanathan V., Crutzen P.J., Kiehl J.T. and Rosenfeld D.: Aerosols, climate, and the hydrological cycle, Science, 294, 2119-2124, https://doi.org/10.1126/science.1064034, 2001.

Rose D., Gunthe S.S., Mikhailov E., Frank G.P., Dusek U., Andreae M.O. and Pöschl U.: Calibration and measurement uncertainties of a continuous-flow cloud condensation nuclei counter (DMT-CCNC): CCN activation of ammonium sulfate and sodium chloride aerosol particles in theory and experiment, Atmos. Chem. Phys., 8, 1153-1179, https://doi.org/10.5194/acp-8-1153-2008, 2008.

Schmale J., Henning S., Decesari S., Henzing B., Keskinen H., Sellegri K., Ovadnevaite J., Pöhlker M.L., Brito J., Bougiatioti A., Kristensson A., Kalivitis N., Stavroulas I., Carbone S., Jefferson A., Park M., Schlag P., Iwamoto Y., Aalto P., Äijälä M., Bukowiecki N., Ehn M., Frank G., Fröhlich R., Frumau A., Herrmann E., Herrmann H., Holzinger R., Kos G., Kulmala M., Mihalopoulos N., Nenes A., O'Dowd C., Petäjä T., Picard D., Pöhlker C., Pöschl U., Poulain L., Prévôt A.S.H., Swietlicki E., Andreae M.O., Artaxo P., Wiedensohler A., Ogren J., Matsuki A., Yum S.S., Stratmann F., Baltensperger U. and Gysel M.: Long-term cloud condensation nuclei number concentration, particle number size distribution and chemical composition measurements at regionally representative

带格式的: 字体: (默认) Times New Roman

带格式的: 字体: (默认) Times New Roman

带格式的: 字体: (默认) Times New Roman, (中文) +中文正文 (等线), 10 磅, 英语(美国)

带格式的: 字体: (默认) Times New Roman, (中文) +中文正文 (等线), 10 磅, 英语(美国)

带格式的: 字体: (默认) Times New Roman, (中文) +中文正文 (等线), 10 磅, 英语(美国)

observatories, Atmos Chem Phys, 18, 2853-2881, https://doi.org/10.5194/acp-18-2853-2018, 2018.
Stock M., Cheng Y.F., Birmili W., Massling A., Wehner B., Müller T., Leinert S., Kalivitis N., Mihalopoulos N. and Wiedensohler A.: Hygroscopic properties of atmospheric aerosol particles over the Eastern Mediterranean: implications for regional direct radiative forcing under clean and polluted conditions, Atmos. Chem. Phys., 11, 4251-4271, https://doi.org/10.5194/acp-11-4251-2011, 2011.
Stokes R.H. and Robinson R.A.: Interactions in aqueous nonelectrolyte solutions. I. Solute-solvent equilibria, The Journal of Physical Chemistry, 70, 2126-2131, 1966.
Stolzenburg M.R. and McMurry P.H.: Equations governing single and tandem DMA configurations and a new lognormal approximation to the transfer function, Aerosol Sci. Tech., 42, 421-432, http://dx.doi.org/10.1080/02786820802157823, 2008.
Stolzenburg M.R. and McMurry P.H.: TDMAFIT user's manual, University of Minnesota, Department of Mechanical Engineering, Particle Technology Laboratory, Minneapolis, 1-61, 1988.
Sun Y., Wang Z., Dong H., Yang T., Li J., Pan X., Chen P. and Jayne J.T.: Characterization of summer organic and inorganic aerosols in Beijing, China with an Aerosol Chemical Speciation Monitor, Atmos. Environ., 51, 250-259, https://doi.org/10.1016/j.atmosenv.2012.01.013, 2012.
Swietlicki E., Hansson H.C., HÄMeri K., Svenningsson B., Massling A., McFiggans G., McMurry P.H., PetÄJÄ T., Tunved P., Gysel M., Topping D., Weingartner E., Baltensperger U., Rissler J., Wiedensohler A. and Kulmala M.: Hygroscopic properties of submicrometer atmospheric aerosol particles measured with H-TDMA instruments in various environments—a review, Tellus B, 60, 432-469, https://doi.org/10.1111/j.1600-0889.2008.00350.x, 2008.
Tan H., Xu H., Wan Q., Li F., Deng X., Chan P.W., Xia D. and Yin Y.: Design and application of an unattended multifunctional H-TDMA system, J. Atmos. Ocean. Tech., 30, 1136-1148, https://doi.org/10.1175/JTECH-D-12-00129.1, 2013.
Tritscher T., Juranyi Z., Martin M., Chirico R., Gysel M., Heringa M.F., DeCarlo P.F., Sierau B., Prevot A.S.H., Weingartner E. and Baltensperger U.: Changes of hygroscopicity and morphology during ageing of diesel soot, Environ. Res. Lett., 6, https://doi.org/10.1088/1748-9326/6/3/034026, 2011.
Twomey S.: Pollution and the planetary albedo, Atmos. Environ., 8, 1251-1256, 1974.
Ulbrich I.M., Canagaratna M.R., Zhang Q., Worsnop D.R. and Jimenez J.L.: Interpretation of organic components from Positive Matrix Factorization of aerosol mass spectrometric data, Atmos. Chem. Phys., 9, 2891-2918, https://doi.org/10.5194/acp-9-2891-2009, 2009.
Wang L.T., Wei Z., Yang J., Zhang Y., Zhang F.F., Su J., Meng C.C. and Zhang Q.: The 2013 severe haze over southern Hebei, China: model evaluation, source apportionment, and policy implications, Atmos. Chem. Phys., 14, 3151-3173, https://doi.org/10.5194/acp-14-3151-2014, 2014.
Wang Y., Zhang F., Li Z., Tan H., Xu H., Ren J., Zhao J., Du W. and Sun Y.: Enhanced hydrophobicity and volatility of submicron aerosols under severe emission control conditions in Beijing, Atmos. Chem. Phys., 17, 5239-5251, https://doi.org/10.5194/acp-17-5239-2017, 2017.
Wang Z., Wu Z., Yue D., Shang D., Guo S., Sun J., Ding A., Wang L., Jiang J. and Guo H.: New particle formation in China: Current knowledge and further directions, Sci. Total Environ., 577, 258-266, https://doi.org/10.1016/j.scitotenv.2016.10.177, 2017.
Wu Z.J., Zheng J., Shang D.J., Du Z.F., Wu Y.S., Zeng L.M., Wiedensohler A. and Hu M.: Particle hygroscopicity and its link to chemical composition in the urban atmosphere of Beijing, China, during summertime, Atmos. Chem. Phys., 16, 1123-1138, https://doi.org/10.5194/acp-16-1123-2016, 2016.

带格式的: 字体: (默认) Times New Roman, (中文) +中文正文 (等线), 10 磅, 英语(美国)

带格式的: 字体: (默认) Times New Roman

带格式的: 字体: (默认) Times New Roman

带格式的: 字体: (默认) Times New Roman

带格式的: 字体: (默认) Times New Roman

Ye X., Tang C., Yin Z., Chen J., Ma Z., Kong L., Yang X., Gao W. and Geng F.: Hygroscopic growth of urban aerosol particles during the 2009 Mirage-Shanghai Campaign, Atmos. Environ., 64, 263-269, https://doi.org/10.1016/j.atmosenv.2012.09.064, 2013.

Zhang F., Li Y., Li Z., Sun L., Li R., Zhao C., Wang P., Sun Y., Liu X., Li J., Li P., Ren G. and Fan T.: Aerosol hygroscopicity and cloud condensation nuclei activity during the AC^{3}Exp campaign: implications for cloud condensation nuclei parameterization, Atmos. Chem. Phys., 14, 13423-13437, https://doi.org/10.5194/acp-14-13423-2014, 2014.

Zhang F., Li Z., Li Y., Sun Y., Wang Z., Li P., Sun L., Wang P., Cribb M., Zhao C., Fan T., Yang X. and Wang Q.: Impacts of organic aerosols and its oxidation level on CCN activity from measurement at a suburban site in China, Atmos. Chem. Phys., 16, 5413-5425, https://doi.org/10.5194/acp-16-5413-2016, 2016.

Zhang F., Wang Y., Peng J., Ren J., Collins D., Zhang R., Sun Y., Yang X. and Li Z.: Uncertainty in predicting CCN activity of aged and primary aerosols, J. Geophys. Res.-Atmos., 122, https://doi.org/10.1002/2017JD027058, 2017.

Zhang Y., Du W., Wang Y., Wang Q., Wang H., Zheng H., Zhang F., Shi H., Bian Y., Han Y., Fu P., Canonaco F., Prévôt, A.S.H., Zhu T., Wang P., Li Z. and Sun Y.: Aerosol chemistry and particle growth events at an urban downwind site in the North China Plain, Atmos. Chem. Phys. Discuss., 2018, 1-29, https://doi.org/10.5194/acp-2017-889, 2018.

Zhang R., Khalizov A.F., Pagels J., Zhang D., Xue H. and McMurry P.H.: Variability in morphology, hygroscopicity, and optical properties of soot aerosols during atmospheric processing, Proceedings of the National Academy of Sciences, 105, 10291-10296, https://doi.org/10.1073/pnas.0804860105,2008.

Zhang R., Wang L., Khalizov A.F., Zhao J., Zheng J., McGraw R.L. and Molina L.T.: Formation of nanoparticles of blue haze enhanced by anthropogenic pollution, Proceedings of the National Academy of Sciences, 106, 17650-17654, https://doi.org/10.1073/pnas.0910125106, 2009.

Zhang S.L., Ma N., Kecorius S., Wang P.C., Hu M., Wang Z.B., Größ J., Wu Z.J. and Wiedensohler A.: Mixing state of atmospheric particles over the North China Plain, Atmos. Environ., 125, Part A, 152-164, https://doi.org/10.1016/j.atmosenv.2015.10.053, 2016.

Zhu Y., Zhang J., Wang J., Chen W., Han Y., Ye C., Li Y., Liu J., Zeng L., Wu Y., Wang X., Wang W., Chen J. and Zhu T.: Distribution and sources of air pollutants in the North China Plain based on on-road mobile measurements, Atmos. Chem. Phys., 16, 12551-12565, https://doi.org/10.5194/acp-16-12551-2016, 2016.

Table 1. The number fractions of different hygroscopic groups for different particle sizes.

	40 nm	80 nm	110 nm	150 nm	200 nm
NH	5.1 %	5.0 %	5.1 %	5.0 %	5.7 %
LH	4.8 %	4.2 %	4.3 %	4.7 %	5.1 %
MH	90.1 %	90.8 %	90.6 %	90.3 %	89.2 %

带格式的: 字体: (默认) Times New Roman, (中文) +中文正文 (等线), 10 磅, 英语(美国)

带格式的: 字体: 10 磅, 字体颜色: 黑色

带格式的: 字体: (默认) Times New Roman, (中文) +中文正文 (等线), 10 磅, 英语(美国)

带格式的: 字体: (默认) Times New Roman, 10 磅, 字体颜色: 黑色

带格式的: 字体: (默认) Times New Roman, (中文) +中文正文 (等线), 10 磅, 英语(美国)

带格式的: 字体: (默认) Times New Roman, (中文) +中文正文 (等线), 10 磅, 英语(美国)

带格式的: 字体: (默认) Times New Roman, (中文) +中文正文 (等线), 10 磅, 英语(美国)

带格式的: 字体: (默认) Times New Roman, (中文) +中文正文 (等线), 10 磅, 英语(美国)

域代码已更改

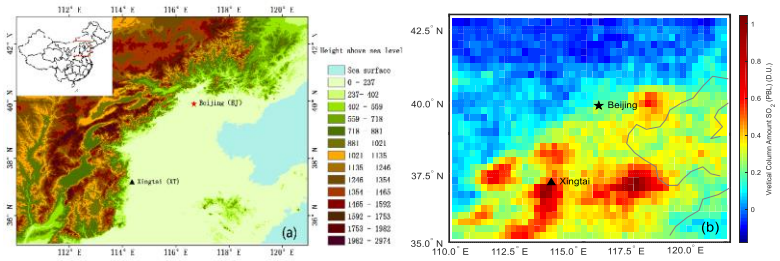

Figure 12. (**a**) Map showing the locations of the sampling sites and (**b**) the distribution of mean SO_2 concentrations off May from 2012 to 2016.

域代码已更改

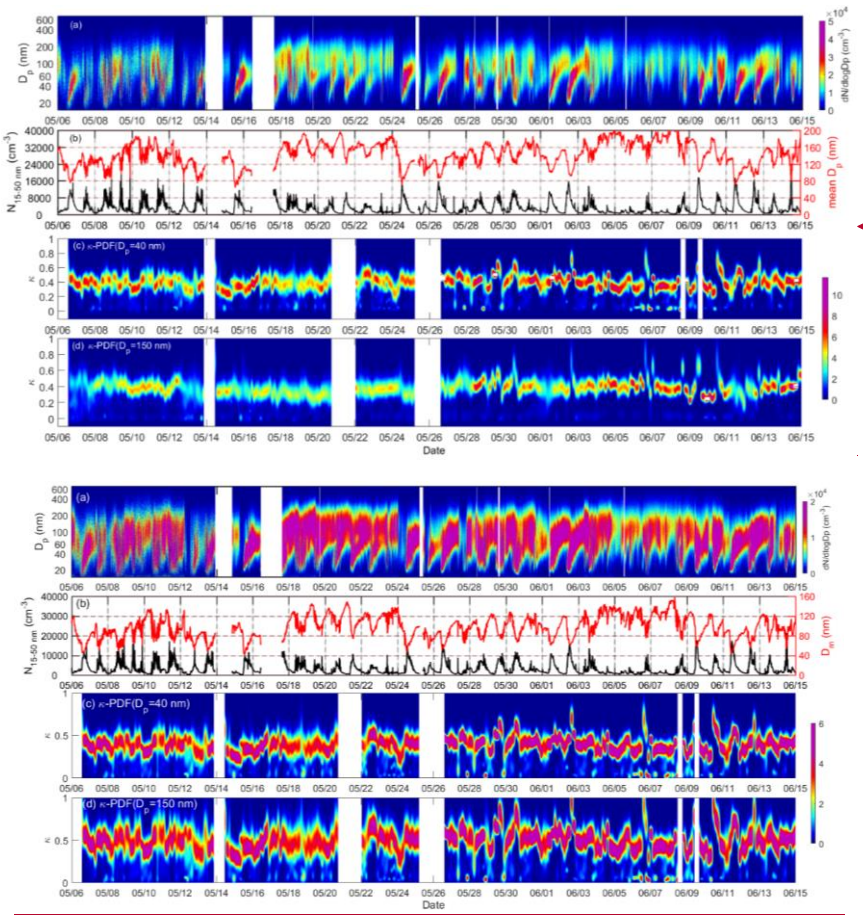

Figure 13. The time series of (**a**) particle number size distribution (PNSD), (**b**) aerosol number concentration in the 15–50 nm range ($N_{15-50\ nm}$) and the geometric mean diameter (D_{mp}), (**c**) the probability density function of κ_{gf} (κ-PDF) for 40 nm and (**d**) 150 nm particles from 6 May to 15 June of 2016.

带格式的: 居中

域代码已更改

带格式的: 字体: (默认) Times New Roman, (中文) 宋体, 12 磅, 字体颜色: 自动设置

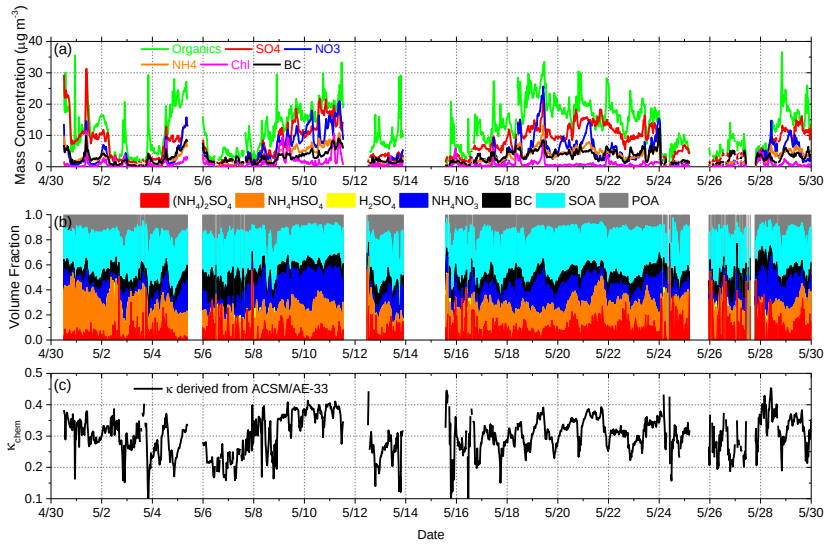

Figure 14. Time series of (**a**) the bulk mass concentration of aerosol species in PM_1, (**b**) the volume fractions of POA, SOA, BC, and inorganics with the simplified ion pairing scheme, and (**c**) the hygroscopicity parameter derived from the chemical compositions (κ_{chem}).

域代码已更改

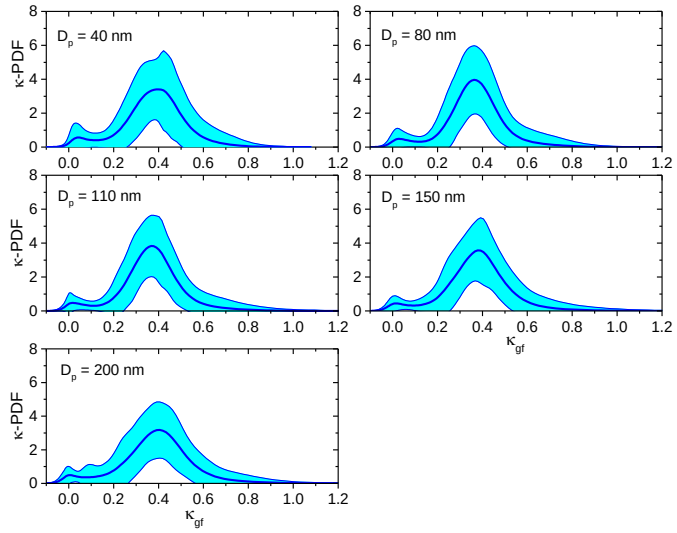

Figure 15. Mean probability density functions of κ_{gf} (κ-PDF) for different particle sizes and their standard deviations (shaded areas) derived from H-TDMA data and measured at RH = 85 %.

域代码已更改

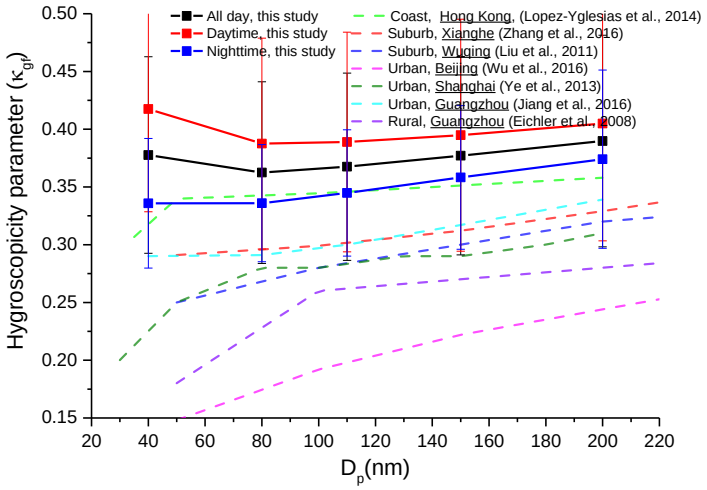

Figure 16. Size-resolved aerosol hygroscopicity parameter (κ_{gf}) derived from H-TDMA data at XT and at other sites in China.

域代码已更改

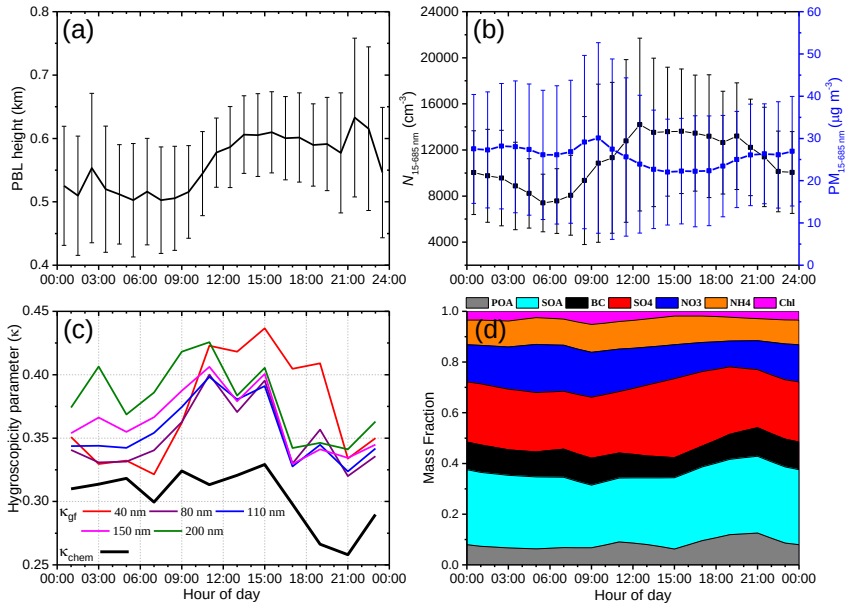

Figure 17. Diurnal variations in (**a**) planetary boundary layer (PBL) height retrieved from the MPL, (**b**) aerosol number and mass concentrations in the 15–685 nm range ($N_{15–685\,nm}$ and $PM_{15–685\,nm}$, respectively) derived from the SMPS (an aerosol density of 1.6 g cm^{-3} is assumed), (**c**) the hygroscopicity parameter derived from the hygroscopic growth factor (κ_{gf}) and predicted from the bulk chemical composition (κ_{chem}), and (**d**) the mass fractions of different species.

域代码已更改

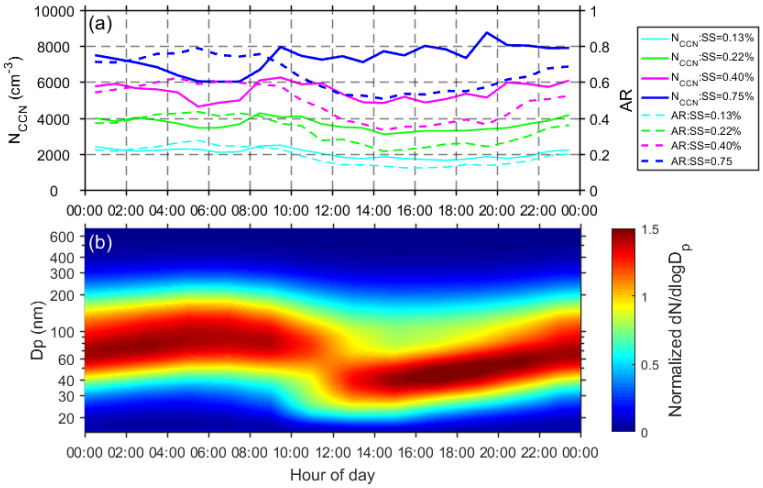

Figure 18. Diurnal variations in (a) CCN number concentration (N_{CCN}) and activation ratio (AR), and (b) the normalized aerosol size distribution in the 15–685 nm particle size range.

域代码已更改

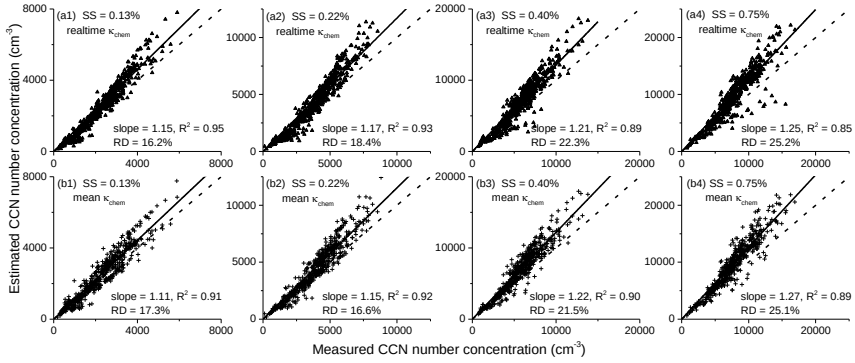

Figure 19. Estimated versus measured CCN number concentration for ambient aerosols at four different supersaturation levels. The N_{CCN} is estimated based on κ-Köhler theory, using the real-time κ_{chem} (**a1-a4**) and the mean κ_{chem} (**b1-b4**). The slope and correlation coefficient (R^2) of the linear regression, and the relative

域代码已更改

deviation of estimated N_{CCN} (RD = $|N_{CCN\_estimated} - N_{CCN\_measured}| / N_{CCN\_measured}$) are shown in each panel. The regression line is overlaid on the measurements (solid line) and the dashed line is the 1:1 line.

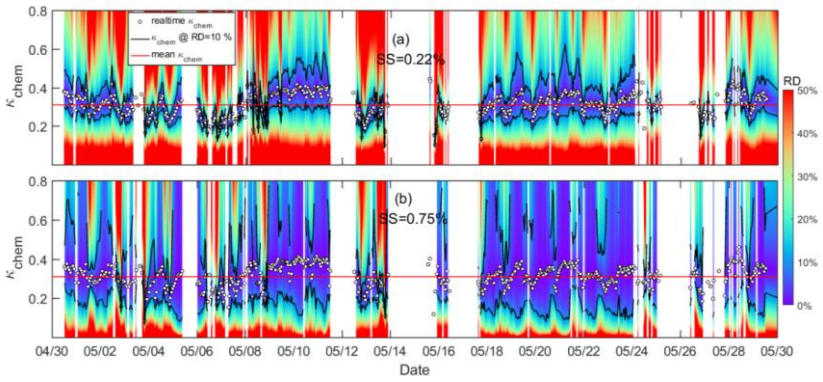

Figure 20. Sensitivity of N_{CCN} estimates to κ_{chem} as a function of time at (a) SS = 0.22 % and (b) SS = 0.75 %. The color scale indicates the relative deviation (RD) of the CCN estimates using the κ_{chem} value shown on the ordinate. In each panel, open circles show the real-time κ_{chem}. Note that RD is by definition zero at these points. The black line is κ at RD = 10 % and the red line is the mean value for κ_{chem} (0.31). Figure ~~S6~~ S8 in the supplement shows the same plots but for SS = 0.13 % and 0.40 %.

域代码已更改